

Instituto Tecnológico y de Estudios Superiores de Monterrey
Campus Monterrey
School of Engineering and Sciences



**TECNOLÓGICO
DE MONTERREY®**

Induced Rotation of Ratchets in Driven Environments

A thesis presented by

Yeray Cruz Ruiz

Submitted to the
School of Engineering and Sciences
in partial fulfillment of the requirements for the degree of

Master
In
Nanotechnology

Monterrey, Nuevo León, México, Nov 2025

Instituto Tecnológico y de Estudios Superiores de Monterrey
Campus Monterrey School of Engineering and Sciences

The committee members, hereby, certify that have read the thesis presented by **Yeray Cruz Ruiz** and that it is fully adequate in scope and quality as a partial requirement for the degree of Master in Nanotechnology.

Antonio Ortiz Ambriz, PhD

Thesis Advisor

School of Engineering Sciences, Tecnológico de Monterrey

Someone, PhD

Sinodal member

Affiliation

Someone, PhD

Sinodal member

Affiliation

Someone, PhD

Sinodal member

Affiliation

Dr. Elisa Virginia Vázquez Lepe
Dean of Graduate Studies
School of Engineering and Sciences
Monterrey, Nuevo León, México, Nov 2025

Declaration of Authorship

I, Yeray Cruz Ruiz (student), declare that this thesis titled, “Induced Rotation of Ratchets in Passive Environments” and the work presented in it are my own. I confirm that:

- This work was done wholly or mainly while in candidature for a research degree at this University.
- Where any part of this thesis has previously been submitted for a degree or any other qualification at this University or any other institution, this has been clearly stated.
- Where I have consulted the published work of others, this is always clearly stated.
- Where I have quoted from the work of others, the source is always given. Apart from such quotations, this thesis is entirely my own work.
- I have acknowledged all main sources of help.
- Where the thesis is based on work done by myself jointly with others, I have made clear exactly what was done by others and what I have contributed myself.

Yeray Cruz Ruiz (Student)
Monterrey, Nuevo León, México, Nov 2025

©2025 by Yeray Cruz Ruiz
All Rights reserved

Dedication

For those who come after.

Acknowledgements

To my parents for their unwavering support, to my friends for making this journey easier, and especially to Dr. Antonio, who always believed in me and was an incredible mentor.

Induced Rotation of Ratchets in Passive Environments

by

Yeray Cruz Ruiz

Abstract

Swimming at the mesoscale has been a topic of growing interest over the past two decades due to the unique dynamics that arise at low Reynolds numbers, a regime where viscous forces dominate over inertial ones. In this environment, motion becomes nonintuitive: as described by the scallop theorem, a swimmer with only one degree of freedom cannot achieve net displacement because its movement is time-reversible under the Navier–Stokes equations. Despite these physical constraints, nature has evolved remarkable strategies to overcome them. Many microorganisms exhibit nonreciprocal motion, allowing them to propel themselves even in highly viscous media. For instance, *Escherichia Coli* uses a rotating flagellum to push fluid backward, propelling the bacterium forward. Inspired by such biological systems, researchers have sought to engineer artificial swimmers capable of movement under similar conditions. One notable example involves bacterial micromotors, where a ratchet-shaped structure is immersed in a bacterial bath. The bacteria, moving along ballistic trajectories, collide with the asymmetric surface of the ratchet, transferring momentum that induces rotation. Over time, however, this motion ceases as the bacteria exhaust the nutrients in their medium, requiring replenishment to sustain activity. This form of active matter relies on energy extracted from its environment. Yet a natural question arises: can we achieve similar directed motion using anisotropically driven—but externally controlled—systems?

In this work, we analyze paramagnetic colloids manipulated by an external precessing magnetic field. The system is confined in the z axis by two glass plates and presents periodic boundary conditions in x , and y axis. When multiple particles are present, dipole-dipole interactions arise, leading to either attraction or repulsion depending on their head-to-tail alignment. The particles' internal magnetic moment also rotate, dynamically altering their interactions over time. We observe that at low frequencies, the colloids form pairs and start rotating with a shared center of mass, whereas from 3.25 to 7Hz particles have a moment of repulsion, creating a neighbor exchange between different pairs, which produce a ballistic trajectory. To investigate whether this motion can perform work, we place a ratchet-like object with different parameters amidst the particles. At the pair rotation frequency regime it was observed how the angular frequency was almost negligible, while in the neighbor exchange regime it can't be described by the thermal noise.

List of Figures

2.1 Example of brownian motion	13
3.1 Feynman ratchet	16
3.2 Ratchet potential examples.	18
3.3 Rocking ratchets experiments.	20
3.4 Lebedev experiment.	21
4.1 Macroscopic Agents example	25
4.2 Artificail microswimmers	29
4.3 MSD for brownian particles	30
4.4 Random Walk for active brownian particles.	31
4.5 Experiments that harness bacteria motility.	34
5.1 Magnetically driven colloids examples.	39
6.1 System overview.	45
6.2 Basic interaction for a pair of paramagnetic colloids.	46
6.3 Dinamycs of paramagnetic colloids in a confined space.	47
6.4 Colloidal states for different packing, height, and frequency.	48
6.5 Representation of the paramagnetic colloids, body-centered-cubic lattice used for the ratchet, and the precessing conic magnetic field.	50
6.6 Workflow diagram.	53
6.7 Ratchet geometry.	54
7.1 Angular velocity as a function of driving frequency.	60
7.2 Particle trajectories at different driving frequencies.	61
7.3 Angular frequency as a function of time.	62
7.4 Histogram of angular frequency.	63
7.5 Angular displacement of a particle.	64

List of Tables

3.1	Summary of operation of ratchet and pawl.	17
6.1	Ratchet physical parameters.	53
6.2	Simulation box physical parameters.	55
6.3	Paramagnetic colloids parameters.	55

Contents

Abstract	vi
List of Figures	vii
List of Tables	ix
I Introduction	1
1 Introduction	3
II Background	5
2 Physics at the mesoscale	7
2.1 Low Renolds Number Regime	7
2.2 Brownian Motion and Thermal Fluctuations	8
2.2.1 Stochastic Representation	8
2.2.2 Velocity Statistics and Energy Equipartition	10
2.2.3 Overdamped Dynamics and Diffussion	11
3 Ratchets and Rectification Mechanisms	15
3.1 The Feynman-Smoluchowski Ratchet	15
3.2 Optical Brownian ratchets	17
4 Active Matter Systems	23
4.1 Fundamentals of Active Matter	23
4.2 Macroscopic Agents	24
4.3 Microscopic Agents	26

4.3.1	Artificial Systems	28
4.3.2	Natural Systems	30
4.4	Obtaining Work from Active Matter	32
5	Magnetically Driven Colloidal Systems	37
III	Methods	43
6	Simulations	45
6.1	Paramagnetic Colloids Dynamics	45
6.2	Molecular Dynamics	47
6.3	Euler-Maruyama Integration Method	51
6.4	Definition of the Solid Ratchet	52
6.5	System Overview and Workflow	53
6.5.1	System's Physical Definition	53
6.5.2	Data Analysis	55
IV	Results	57
7	Results	59
V	Conclusions	65
8	Conclusions	67
Bibliography		69
Curriculum Vitae		79

Part I

Introduction

Chapter 1

Introduction

The study of motion at the microscale lies at the intersection of physics, chemistry, and biology, with implications for both fundamental understanding and technological applications. In this regime, inertia becomes negligible and viscous forces dominate, while random fluctuations from thermal noise play a significant role. Understanding how to control, rectify, and harness such motion has therefore become a central challenge in soft matter and statistical physics [1, 2]. Beyond theoretical curiosity, these ideas underpin innovations in microfluidic devices, targeted drug delivery, and nanoscale engines.

Nature already offers remarkable examples of how microscopic systems can convert energy into directed motion. Within cells, molecular motors such as kinesin and dynein transport cargo along cytoskeletal filaments. On larger biological scales, microorganisms like *E. coli*, sperm cells, and algae have evolved efficient strategies to swim through highly viscous environments [3–5]. The study of these self-propelled entities has led to the emergence of the field of active matter, which explores collections of self-driven units operating far from equilibrium [6–8]. In recent years, this concept has expanded to include collective and emergent behaviors, such as topological flows in active materials [9].

To channel and control this active motion, researchers have drawn inspiration from another concept: ratchets. Ratchets are asymmetric structures or potentials that convert random fluctuations into net directional motion—a principle famously illustrated by Feynman’s thought experiment. Their study has led to the development of Brownian motors, systems that harness thermal or active noise for controlled transport [10, 11]. More recently, these principles have been extended to active matter, where active Brownian particles can be rectified into persistent directional flows [12–14].

A striking realization of this idea was demonstrated by Di Leonardo [15], who showed that asymmetric microgears immersed in dense bacterial suspensions could rotate spontaneously,

powered solely by the activity of *E. coli*. These bacterial ratchets combine nonequilibrium activity with geometric asymmetry to generate mechanical motion without external input. Subsequent studies have revealed that bacterial collisions with curved microstructures can exert measurable forces, and that the curvature of the structure itself can modulate its rotation speed [16]. Together, these results highlight how geometric design and collective active behavior can be harnessed for autonomous transport and mixing at the microscale.

Even with these advances, there are still open problems. Active matter is powerful but not always easy to control or keep stable, since living systems depend strongly on their environment [8]. Passive colloids are easier to handle in experiments but need external driving to move in a directed way. Magnetically driven colloids are promising in this respect because their interactions can be tuned, they are reversible, and they can be controlled externally. Experiments have shown magnetic colloidal carpets that propel and carry cargo [17], and other studies have revealed enhanced diffusion, synchronization, and bidirectional transport under confinement [18–21]. Still, the interplay between confinement, collective effects, and external driving is not fully understood.

This thesis looks at these questions by using numerical simulations of paramagnetic colloids under magnetic fields, with emphasis on confinement and ratchet effects. Simulations are useful because they allow us to test conditions that are hard to achieve in experiments and to separate the roles of noise, interactions, and driving. By studying transport properties, collective effects, and symmetry breaking, we aim to clarify how random microscopic motion can be rectified into useful work. The results connect to basic questions in nonequilibrium systems and may also guide the design of micro- and nanoscale devices, where controlled transport is essential.

The thesis is organized as follows. Part II reviews the theoretical background, including motion at low Reynolds number, Brownian noise, ratchet mechanisms, and the difference between active and passive matter. Part III describes the simulation methods, with focus on stochastic molecular dynamics. Part IV presents the main findings on confined colloidal dynamics and rectification. Finally, Part V summarizes the contributions and suggests future work.

Part II

Background

Chapter 2

Physics at the mesoscale

2.1 Low Reynolds Number Regime

At the mesoscale, where objects such as bacteria and colloidal particles operate, the physical world is governed by a regime in which viscous forces dominate over inertial ones. This regime is characterized by a small Reynolds number (Re), a dimensionless quantity that compares inertial to viscous effects. Therefore, the force applied at that moment will describe the movement or displacement performed, not depending on any past force, this is a characteristic of an over-damped system. In his seminal lecture, Life at Low Reynolds Number [1], Purcell highlighted the surprising and often counterintuitive behaviors that emerge in such environments. For instance, time-reversible motion — common at macroscopic scales — is ineffective for propulsion at low Re , necessitating non-reciprocal strategies like flagellar rotation or body undulation. This leads to the scallop theorem, that states that an object with a single degree of freedom — such as a scallop in a viscous regime — will not have net displacement.

Microswimmers processes can be described by the Navier-Stokes equation without the inertia terms, leaving us without any time depending terms as shown in Eq. (2.1). This has been a topic of interest for researchers that are constantly looking for ways of transportation in those environments for specific tasks. Unfortunately this is not the only challenge we face when moving at the microscale.

$$-\nabla p + \eta \nabla^2 \vec{v} = 0 \tag{2.1}$$

2.2 Brownian Motion and Thermal Fluctuations

Even though this is a viscous regime, particles are not static. At small length scales, such as those of colloidal particles or bacteria, random thermal fluctuations become a dominant source of motion. This phenomenon, known as *Brownian motion*, was first explained quantitatively by Albert Einstein in 1905. He demonstrated that the irregular paths observed in microscopic particles suspended in fluid result from collisions with the molecules of the surrounding medium [2].

Einstein's work provided one of the first convincing arguments for the molecular nature of matter and led to a mathematical description of how these random movements accumulate over time. Specifically, he derived that the mean squared displacement (MSD) of a particle grows linearly with time:

$$\langle x^2(t) \rangle = 2Dt, \quad (2.2)$$

where D is the diffusion coefficient, a measure of how quickly particles spread out. Einstein further related this coefficient to measurable physical parameters through the expression:

$$D = \frac{k_B T}{6\pi\eta R}, \quad (2.3)$$

where k_B is Boltzmann's constant, T the absolute temperature, η the dynamic viscosity of the fluid, and R the radius of the spherical particle. This relation — often referred to as the *Einstein-Stokes equation* — is foundational in soft matter and colloidal physics. In the systems considered in this thesis, Brownian motion plays a crucial role in the dynamics of passive colloids and must be accounted for even in the presence of external fields or active agents, such as bacteria.

While Einstein's formulation captures the long-term diffusive behavior of Brownian particles, it does not account for their instantaneous dynamics. To describe how particles move under both viscous damping and random thermal forces, we turn to a stochastic differential equation known as the *Langevin equation*.

2.2.1 Stochastic Representation

The Langevin equation [22] in one dimension, including inertial effects, damping, and thermal noise, can be written as:

$$m\ddot{x} = F - \gamma\dot{x} + \eta(t), \quad (2.4)$$

where m is the particle mass, γ is the damping coefficient, and $\eta(t)$ is a stochastic force representing thermal noise. For simplicity, we write the velocity as $v = \dot{x}$, leading to:

$$m \frac{dv}{dt} = F - \gamma v + \eta(t). \quad (2.5)$$

Discretizing time with a small step dt , we apply the definition of a derivative:

$$m \frac{v(t+dt) - v(t)}{dt} = F - \gamma v(t) + \eta(t). \quad (2.6)$$

The thermal noise term $\eta(t)$ is modeled as a Gaussian white noise process:

$$\eta(t) dt = g dW, \quad (2.7)$$

where dW is a Wiener increment (increment of Brownian motion) such that:

$$\langle dW \rangle = 0, \quad \langle dW^2 \rangle = dt. \quad (2.8)$$

Solving for $v(t+dt)$ gives:

$$v(t+dt) = v(t) + \frac{dt}{m}(F - \gamma v(t)) + g dW. \quad (2.9)$$

Now, assuming no deterministic force ($F = 0$) — as is the case for free passive particles:

$$v(t+dt) = v(t) - \frac{\gamma dt}{m} v(t) + g dW. \quad (2.10)$$

Taking the expectation value (mean) of both sides:

$$\langle v(t+dt) \rangle = \langle v(t) \rangle - \frac{\gamma dt}{m} \langle v(t) \rangle + g \langle dW \rangle. \quad (2.11)$$

Since $\langle dW \rangle = 0$, the last term vanishes:

$$\langle v(t+dt) \rangle = \langle v(t) \rangle \left(1 - \frac{\gamma dt}{m} \right). \quad (2.12)$$

In the limit of small dt , this leads to the differential equation:

$$\frac{d}{dt} \langle v(t) \rangle = -\frac{\gamma}{m} \langle v(t) \rangle, \quad (2.13)$$

whose solution is:

$$\langle v(t) \rangle = \langle v(0) \rangle e^{-\gamma t/m}. \quad (2.14)$$

This result shows that the average velocity of a particle in a viscous fluid decays exponentially due to damping. This result describes how the velocity decays over time, depending on the mass of the particle and the dynamic drag.

2.2.2 Velocity Statistics and Energy Equipartition

To compute the variance of the velocity, we start again from the Langevin equation in discretized form, without external forces:

$$v(t + dt) = v(t) - \frac{\gamma}{m} v(t) dt + \frac{g}{m} dW. \quad (2.15)$$

Squaring both sides:

$$v(t + dt)^2 = \left[v(t) - \frac{\gamma}{m} v(t) dt + \frac{g}{m} dW \right]^2, \quad (2.16)$$

$$\begin{aligned} &= v(t)^2 + \left(\frac{\gamma}{m} \right)^2 v(t)^2 dt^2 + \left(\frac{g}{m} \right)^2 dW^2 \\ &\quad - 2 \frac{\gamma}{m} v(t)^2 dt + 2 \frac{g}{m} v(t) dW - 2 \frac{\gamma g}{m^2} v(t) dW. \end{aligned} \quad (2.17)$$

Now we take the expectation value:

$$\begin{aligned} \langle v(t + dt)^2 \rangle &= \langle v(t)^2 \rangle + \left(\frac{\gamma}{m} \right)^2 \langle v(t)^2 \rangle dt^2 + \left(\frac{g}{m} \right)^2 \langle dW^2 \rangle \\ &\quad - 2 \frac{\gamma}{m} \langle v(t)^2 \rangle dt + 2 \frac{g}{m} \langle v(t) \rangle \langle dW \rangle - 2 \frac{\gamma g}{m^2} \langle v(t) \rangle \langle dW \rangle. \end{aligned} \quad (2.18)$$

Using the properties of the Wiener process Eq. 2.12, and neglecting second-order small terms (dt^2), we obtain:

$$\langle v(t + dt)^2 \rangle = \langle v(t)^2 \rangle + \frac{g^2}{m^2} dt - 2 \frac{\gamma}{m} \langle v(t)^2 \rangle dt. \quad (2.19)$$

Taking the continuous limit:

$$\frac{d}{dt} \langle v(t)^2 \rangle = -2 \frac{\gamma}{m} \langle v(t)^2 \rangle + \frac{g^2}{m^2}. \quad (2.20)$$

This is a linear first-order ODE. Solving it with variation of constants yields:

$$\langle v(t)^2 \rangle = \frac{g^2}{2\gamma m} + D e^{-2\gamma t/m}. \quad (2.21)$$

As $t \rightarrow \infty$, the exponential term vanishes and we get the stationary value:

$$\lim_{t \rightarrow \infty} \langle v(t)^2 \rangle = \frac{g^2}{2\gamma m}. \quad (2.22)$$

From the equipartition theorem [23], we know that the average kinetic energy is:

$$\frac{1}{2}m\langle v^2 \rangle = \frac{1}{2}k_B T.$$

Therefore:

$$\langle v^2 \rangle = \frac{k_B T}{m}. \quad (2.23)$$

Matching this to our stochastic result:

$$\frac{k_B T}{m} = \frac{g^2}{2\gamma m} \Rightarrow g^2 = 2\gamma k_B T, \quad g = \sqrt{2\gamma k_B T}. \quad (2.24)$$

This defines the noise amplitude in terms of temperature, viscosity, and Boltzmann's constant, parameters that are primordial when defining a system.

2.2.3 Overdamped Dynamics and Diffusion

In the overdamped limit, inertia is negligible, so the Langevin equation becomes:

$$0 = F - \gamma \frac{dx}{dt} + \eta(t). \quad (2.25)$$

Solving for the velocity:

$$\frac{dx}{dt} = \frac{1}{\gamma}(F + \eta(t)). \quad (2.26)$$

For free diffusion ($F = 0$):

$$\frac{dx}{dt} = \frac{1}{\gamma}\eta(t). \quad (2.27)$$

Using stochastic calculus with $\eta(t)dt = gdW$, we write:

$$x(t + dt) = x(t) + \frac{g}{\gamma}dW. \quad (2.28)$$

Mean Position Taking the expectation value:

$$\langle x(t + dt) \rangle = \langle x(t) \rangle + \frac{g}{\gamma}\langle dW \rangle = \langle x(t) \rangle. \quad (2.29)$$

So the mean position remains constant in free diffusion.

Mean Square Displacement (MSD) Squaring the position update:

$$x(t+dt)^2 = x(t)^2 + 2\frac{g}{\gamma}x(t)dW + \left(\frac{g}{\gamma}\right)^2 dW^2. \quad (2.30)$$

Taking the expectation:

$$\langle x(t+dt)^2 \rangle = \langle x(t)^2 \rangle + 2\frac{g}{\gamma} \langle x(t) \rangle \langle dW \rangle + \frac{g^2}{\gamma^2} \langle dW^2 \rangle, \quad (2.31)$$

$$= \langle x(t)^2 \rangle + \frac{g^2}{\gamma^2} dt. \quad (2.32)$$

In differential form:

$$\frac{d}{dt} \langle x(t)^2 \rangle = \frac{g^2}{\gamma^2}. \quad (2.33)$$

Using $g^2 = 2\gamma k_B T$, we substitute:

$$\frac{d}{dt} \langle x(t)^2 \rangle = \frac{2k_B T}{\gamma}. \quad (2.34)$$

Integrating gives the mean squared displacement (MSD):

$$\langle x(t)^2 \rangle = \frac{2k_B T}{\gamma} t. \quad (2.35)$$

This is the classical diffusion result, where the diffusion coefficient is $D = \frac{k_B T}{\gamma}$, consistent with Einstein's expression.

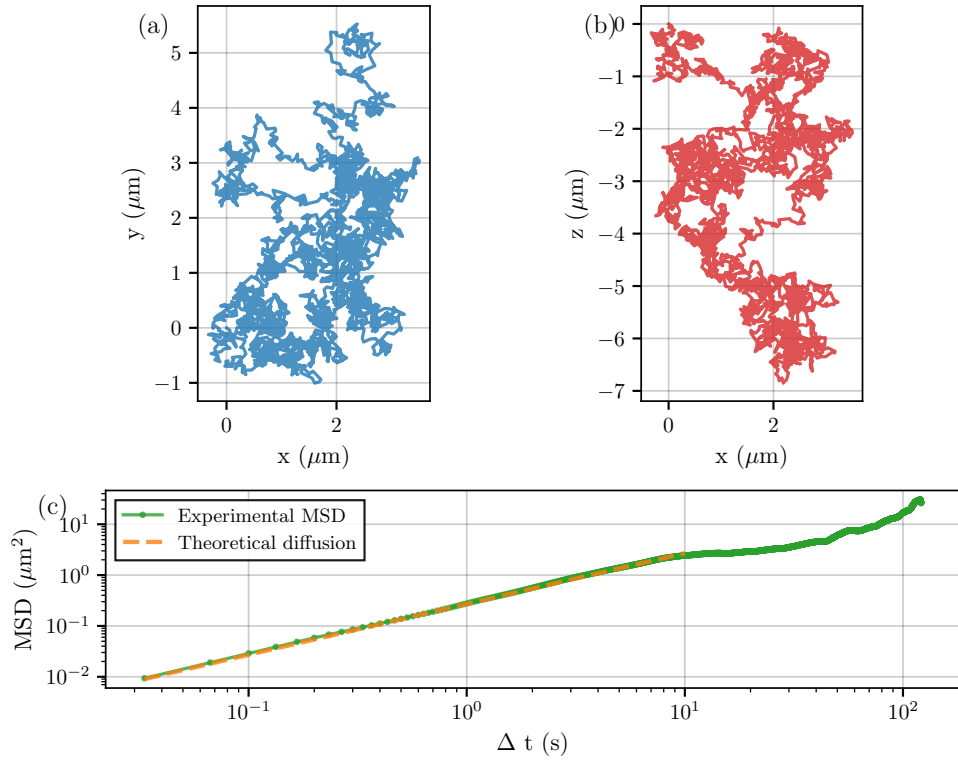


Figure 2.1: A colloidal particle undergoes random, thermally induced displacements in a fluid medium. **Panel a) and b)** shows the trajectory of the particle. **Panel c)** shows the corresponding mean squared displacement (MSD) as a function of time, illustrating the linear relationship predicted by Einstein for diffusive behavior (orange) and the one obtained through a numerical simulation (blue).

Chapter 3

Ratchets and Rectification Mechanisms

3.1 The Feynman-Smoluchowski Ratchet

The inherent randomness of Brownian motion naturally leads to the question: can this disorder be transformed into order? In other words, can the random thermal motion of particles be used to produce directed movement or extract work? This question sits at the core of statistical mechanics and was famously explored by Richard Feynman in his lectures on physics, through a thought experiment known as the Feynman ratchet and pawl [24].

The Feynman ratchet consists of a set of vanes connected to a ratchet wheel, immersed in a fluid (Fig. 3.1). The idea is: random collisions from the surrounding molecules could push the vanes, but the pawl only allows rotation in one direction. At first glance, this asymmetric mechanism seems capable of converting random thermal motion into unidirectional rotation, apparently violating the second law of thermodynamics.

However, Feynman's analysis showed that when both the ratchet and the pawl are in thermal equilibrium with the same heat bath, the system cannot produce net work. The pawl itself undergoes thermal fluctuations and can occasionally lift off, allowing the ratchet to move backward. Over time, the forward and backward movements average out, and no net rotation occurs. This result reinforces the principle that thermal fluctuations alone cannot be rectified to perform work without a temperature gradient or an external energy input.

Despite this limitation, the Feynman ratchet introduced a powerful concept: asymmetry combined with non-equilibrium conditions can, in principle, produce directed motion. This idea is foundational in the study of Brownian motors, biomolecular machines, and active matter systems, including the systems explored in this thesis. In such systems, energy is continuously supplied, whether through bacterial metabolism or magnetic field modulation, creating the necessary non-equilibrium environment that allows motion rectification to occur.



Figure 3.1: Visual representation of the Feynman ratchet. Obtained from [24]

The failure of the Feynman ratchet in thermal equilibrium is intimately connected to another famous thought experiment: Maxwell’s demon. Both systems attempt to extract work from thermal fluctuations through selective processes—the ratchet through mechanical asymmetry, and the demon through information gathering.

Maxwell’s demon, proposed in 1867, imagines a microscopic being that can sort fast and slow molecules between two chambers, creating a temperature difference without apparent work. Similarly, the pawl in Feynman’s ratchet acts as a mechanical “demon,” attempting to select only forward fluctuations while blocking backward motion. However, both fail for the same fundamental reason: the cost of selection itself [25, 26]. Brillouin [27] and later Landauer [28] showed that Maxwell’s demon must expend energy to measure molecular velocities and erase information, with the minimum energy cost being $kT \ln 2$ per bit erased. In the Feynman ratchet, the pawl must “decide” whether to allow motion, and this decision-making process — manifested as thermal fluctuations of the pawl itself — has an entropic cost that exactly cancels any work extracted.

This connection reveals a deep principle: rectification requires either an information gradient (knowledge about the system) or an energy gradient (non-equilibrium conditions). As Parrondo and Español [29] demonstrated, the Feynman ratchet can be viewed as an information engine where the pawl performs measurements on the ratchet’s position. When the pawl and ratchet are at the same temperature, the information gained equals the entropy produced, yielding no net work.

Table 3.1: Summary of operation of ratchet and pawl. Obtained from [24]

Forward:	Needs energy	$\epsilon + L\theta$ from vane. \therefore Rate = $\frac{1}{\tau} e^{-(L\theta+\epsilon)/kT_1}$
	Takes from vane	$L\theta + \epsilon$
	Does work	$L\theta$
	Gives to ratchet	ϵ
Backward:	Needs energy	ϵ for pawl. \therefore Rate = $\frac{1}{\tau} e^{-\epsilon/kT_2}$
	Takes from ratchet	ϵ
	Releases work	$L\theta$
	Gives to vane	$L\theta + \epsilon$

If system is reversible, rates are equal, hence

$$\frac{\epsilon + L\theta}{T_1} = \frac{\epsilon}{T_2}.$$

$$\frac{\text{Heat to ratchet}}{\text{Heat from vane}} = \frac{\epsilon}{L\theta + \epsilon}. \quad \text{Hence} \quad \frac{Q_2}{Q_1} = \frac{T_2}{T_1}.$$

3.2 Optical Brownian ratchets

While Feynman's ratchet fails due to thermal equilibrium, rectified motion becomes possible when detailed balance is broken through external driving. Magnasco [30] demonstrated this principle through the "rocking ratchet" mechanism. In his model, a Brownian particle moves in an asymmetric periodic potential — essentially a sawtooth-shaped energy landscape with gentle slopes in one direction and steep walls in the other. The crucial innovation was applying an oscillating force $F(t) = A \cos(\omega t)$ that rocks the potential back and forth. Although this force has zero time average—pushing equally left and right—the combination with the spatial asymmetry produces net directional motion. When the force tilts the potential forward, particles easily climb the gentle slopes and can overcome barriers. When tilted backward, particles encounter steep walls and remain trapped. This asymmetric response to symmetric driving breaks the forward-backward symmetry of thermal diffusion.

This mechanism differs fundamentally from Feynman's original ratchet: rather than attempting to rectify equilibrium fluctuations (which violates the second law), the rocking ratchet con-

tinuously injects energy through the oscillating force. The time-dependent driving maintains the system far from equilibrium, enabling the spatial asymmetry to generate directed transport. This principle—that asymmetry plus non-equilibrium driving yields rectification—underlies numerous biological processes and provides the theoretical foundation for the magnetically-driven ratchets explored in this thesis.

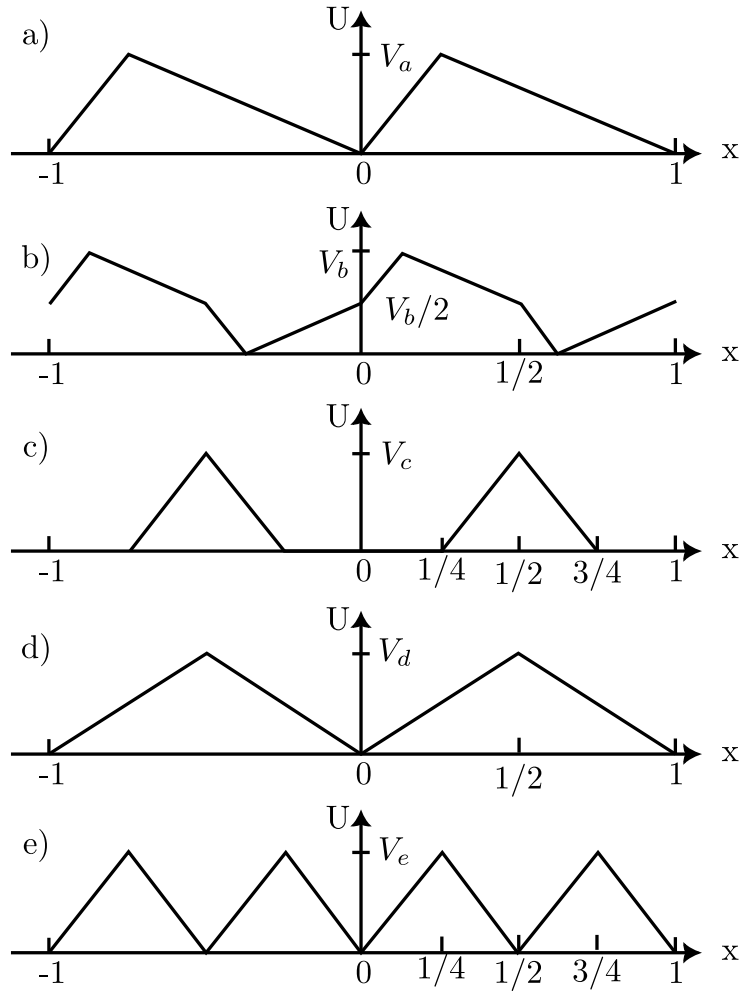


Figure 3.2: Example of ratchet potentials reconstructed from [31]. **Panel a) and b)** show asymmetric potentials, the remaining are symmetric.

Following Magnasco's rocking ratchet where an oscillating force drives particles in a static potential, Ajdari [32] analyzed rectification in periodic structures with either spatial or temporal asymmetry. Using a sawtooth potential with asymmetric slopes (steep of height ϵ/a and gentle of ϵ/b), they identified distinct transport regimes as a function of the AC force amplitude γ . For

small forces $\gamma < \epsilon/a$, particles remain trapped. In the intermediate regime $\epsilon/a < \gamma < \epsilon/b$, rectification occurs as particles can climb the gentle slope but not the steep one, yielding either integer velocities $V = n$ when particles fully relax between cycles, or rational velocities $V = n - 1/(m + 1)$ when incomplete relaxation creates a periodic pattern over multiple cycles.

This concept was later demonstrated experimentally by Faucheux [33], who created an "optical thermal ratchet" using focused laser beams. To generate a circular trap without introducing external forces, they passed the laser through a plate to create circular polarization, maintaining constant laser intensity along the circular path. By rotating the laser beam fast enough, particles could not experience any directed force from the beam itself, allowing them to move freely. They modulated the beam intensity to create an asymmetric potential mimicking a ratchet shape, as shown in Figure 3.3 panel b). They observed that particles localized in potential minima when the modulation was turned on, while for sufficiently long periods, particles moved either backward or forward with equal probability.

A different approach was developed by Lee [34] who employed holographic optical trapping with a symmetric potential. Their system consisted of discrete optical tweezers functioning as potential wells. This approach consisted of turning the potential on and off, displace the trap, and turning it on again, calling each displaced potential a state. Between each state — when the potential is off —, particles are released and free to diffuse, nevertheless they can rapidly jump between adjacent traps. Using this methodology, they achieved net particle displacement in one direction, as illustrated in Figure 3.3 panel a). Remarkably, when they reversed the direction of well displacement, particles followed the trap movement in the opposite direction. Due to this predictable response to trap motion, they named this system a "deterministic thermal ratchet."

Lebedev [36] modified this approach to manipulate rubidium atomic clouds by using three linearly polarized beams acting only in the xy-plane, as shown in Figure 3.4. They applied forces to particles by phase-modulating two of the three lasers, which shifts the entire optical lattice. The modulation was generated using RF generators to produce potentials V_x and V_y . The sum $V_x + V_y$ served as the input signal for beam 2, while the difference $V_x - V_y$ was used for beam 3, creating the rocking forces. They studied this system using ultracold rubidium atoms as test particles. To track the atomic positions, they employed a CCD camera to determine the center of mass of the atomic cloud.

In their first experiment, they applied a biharmonic drive along only one axis. As expected, the system reduced to a one-dimensional harmonic ratchet, and they observed directed particle motion along the axis of the applied biharmonic force. In subsequent experiments, they applied harmonic drives along both axes, with one frequency being twice the other. Their results showed that particles experienced directed motion along the axis with the faster harmonic, while motion

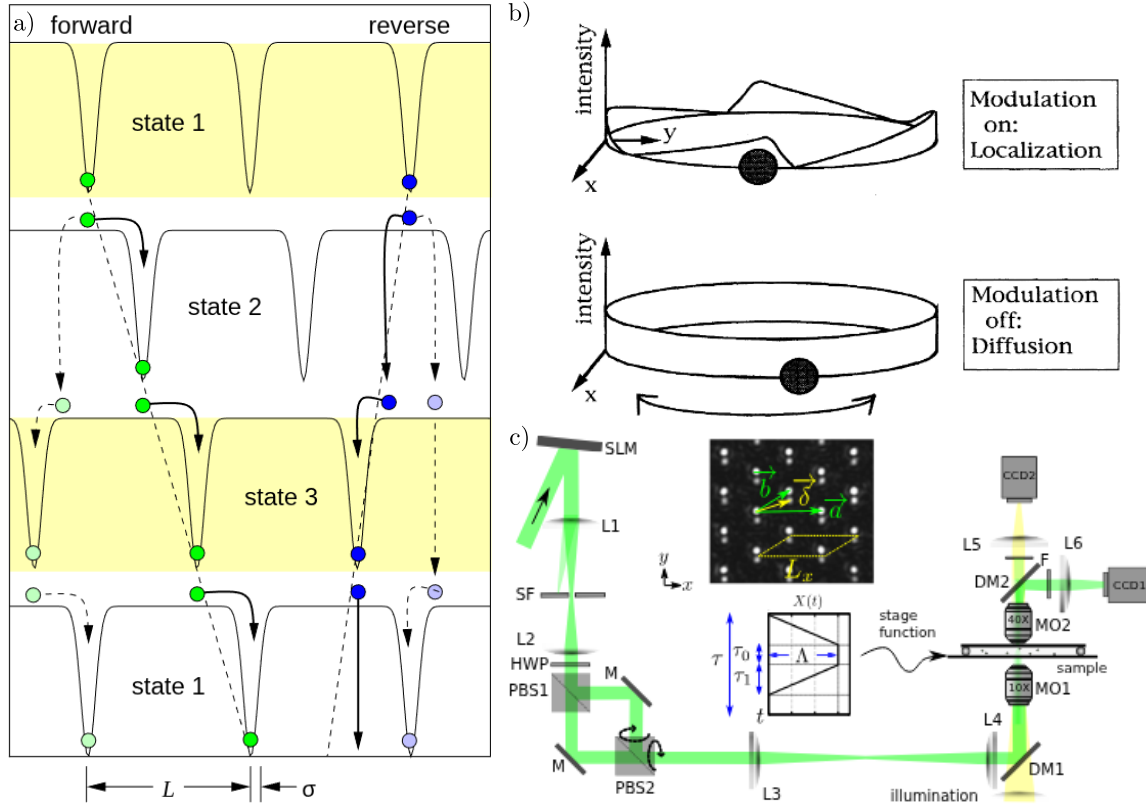


Figure 3.3: **Panel a)** Discrete pattern of optical traps with displacement in one direction, minimum width of σ and a maximum width of L . Obtained from [34]. **Panel b)** When the modulation is on, the beam intensity follows the shape of a ratchet potential with 4 periods per cycle. When the modulation is off, the intensity remains constant, allowing particles to diffuse freely. Obtained from [33]. **Panel c)** Experimental setup of the spatial light modulator, upper inset shows the basis vectors (\vec{a} and \vec{b}) of the main lattice and the displacement for the clone lattice ($\vec{\delta}$), the lower inset illustrates the movement amplitude of the stage, obtained from [35]

along the other axis remained diffusive. In their final experiment, they applied biharmonic drives simultaneously along both axes to investigate whether directed transport could be achieved in two dimensions. By varying the relative weights of the forces along each axis, they demonstrated that it was possible to control the atomic displacement and direct atoms to specific target positions as shown in Figure 3.4 b).



Figure 3.4: **Panel a)** Lattice beam configuration in the xy plane. $\theta = 60^\circ$. **Panel b)** Position of the atomic cloud center of mass at different instants and forces when applying biharmonic at the same time in xy-plane. Obtained from [36].

Following the same lattice-based approach, Arzola [35] successfully recreated all five two-dimensional Bravais lattices using computer-generated holographic optical micromanipulation. Their potential consisted of Gaussian wells distributed along a primary lattice, combined with a shifted replica of the same lattice with a reduced depth factor, Q, compared to the original. The asymmetry of the resulting potential depended directly on both the depth factor Q and the displacement between the original and replica lattices. They implemented the rocking mechanism by moving the particle cell along one axis, as shown in Figure 3.3 c).

The researchers performed three main experiments to validate their results, each with three different diffusion parameters (including no diffusion as one condition), calculating the current in the x and y axes with respect to the amplitude of movement. In the first experiment, they set the asymmetry parallel to the rocking force. They observed that since the wells were aligned with the particle movement, particles tended to move in the direction of the force, traveling from well to well, while experiencing no movement in the perpendicular direction. Current was present along the entire amplitude range. The second experiment positioned the asymmetry perpendicular to the rocking force direction, yielding interesting results. Similar to the first experiment, current

appeared along only one axis (the asymmetry axis), but the current behaved like a Gaussian bell curve. When the rocking movement amplitude approached the asymmetry lattice spacing, particles only moved back and forth between two wells in the x direction, experiencing no current in the y axis. For the final experiment, they examined how the system behaved under a combination of both previous configurations. They created an oblique lattice with the asymmetry aligned with the rocking force direction, producing an oblique particle current. The results were essentially a combination of the two previous experiments: at certain amplitudes, current appeared in both axes, but as amplitude increased, the y-axis current decreased while the x-axis current increased.

Feynman demonstrated that a purely thermal Brownian ratchet cannot generate directed motion due to the second law of thermodynamics. However, introducing specific conditions to break symmetry has proven ideal for bypassing these limitations. One successful approach to achieving this symmetry breaking involves rocking ratchets, where an external periodic drive is applied to an asymmetric potential. Previous experiments have demonstrated the potential of optics to create such asymmetries with high precision and control. While obtaining directed motion at the microscale remains challenging, by applying these symmetry-breaking parameters it becomes possible not only to overcome thermal noise but to harness it for directional transport. Unfortunately, as shown in previous works, implementing these systems often requires specific and sophisticated experimental setups. Interestingly, nature has already developed an alternative solution by creating matter capable of self-propulsion, known as active matter, which achieves directed motion through entirely different mechanisms.

Chapter 4

Active Matter Systems

4.1 Fundamentals of Active Matter

The definition of active matter is not always the same across the literature. Some authors describe it in a broad way, emphasizing that the key element is the continuous intake and dissipation of energy by each unit, which allows them to remain out of equilibrium and sustain motion or internal stresses. Reviews often highlight internally driven systems—such as cytoskeletal extracts, swimming microorganisms, or synthetic colloids—as the most representative examples of active matter [5, 6, 8].

Other authors focus more specifically on self-propulsion at the particle level as the defining feature. This perspective is useful for distinguishing active systems from those whose dynamics are mainly caused by externally imposed forces. For example, in vibrated granular monolayers, asymmetric grains can display self-propelled trajectories and flock-like patterns and are sometimes described as active. In contrast, symmetric grains that only move in a directed way because of an asymmetric boundary, such as a sawtooth channel, are better classified as externally driven rather than active [37–39]. There is also a difference when considering individual vs. collective behavior. Some colloids appear passive when studied alone, but when interactions are taken into account, they can exhibit genuinely non-equilibrium collective phenomena. Examples include motility-induced phase separation (MIPS), defect-mediated flows in active nematics, and other emergent patterns normally linked with active matter. For this reason, several reviews describe active matter not only in terms of single-particle propulsion but also in terms of its collective stresses and patterns [40, 41].

Simple theoretical models have played a crucial role in understanding active matter. One of the best-known examples is the Vicsek model, which shows how local alignment rules together with noise can lead to large-scale collective motion from basic self-driven units [42, 43]. At the

level of single particles, the Active Brownian Particle model is a common way to study colloidal swimmers. In this model, motion is explained by a constant propulsion force, combined with random changes in orientation resulting from rotational diffusion [44, 45].

More recent works point out that definitions have evolved over time and suggest clarifying criteria such as whether the drive is internal or external, whether the system is dry or wet (momentum non-conserving or conserving), and whether the energy input acts at the particle level. Some surveys even propose that researchers explicitly state their working definition depending on the context of their problem [46, 47].

Working definition. In this thesis, we define active matter as:

systems composed of units that continuously draw energy at the particle scale and convert it into mechanical work, generating persistent stresses or self-propulsion, and sustaining non-equilibrium collective dynamics.

This definition includes both biological and synthetic systems (such as bacteria, cytoskeletal extracts, and Janus colloids) but excludes setups where directed motion arises only from externally imposed vibrations or asymmetric boundaries without particle-level energy input—for example, symmetric grains transported by a sawtooth channel [11, 48].

We will first present some macroscopic examples that show universal principles of self-organization, and then move to the microscopic cases most relevant to this work—active colloids, run-and-tumble swimmers, and active nematics—where thermal noise and low-Reynolds-number hydrodynamics play a dominant role.

4.2 Macroscopic Agents

Examples of active matter can be observed at plain sight in the macroscopic world. A flock of birds, for instance, is considered active matter because each bird is capable of self-propulsion. Unlike microscopic systems, they are not significantly affected by the thermal noise of their medium—in this case, air. A computational study by Reynolds [49] modeled flocking behavior in birds by treating each individual as an autonomous agent whose trajectory was influenced by its local environment and neighboring individuals.

Reynolds introduced three fundamental rules governing flocking behavior: separation (collision avoidance), alignment (velocity matching with neighbors), and cohesion (attraction toward the average position of neighbors). This work laid the foundation for understanding how simple local interactions can give rise to complex patterns of collective motion.

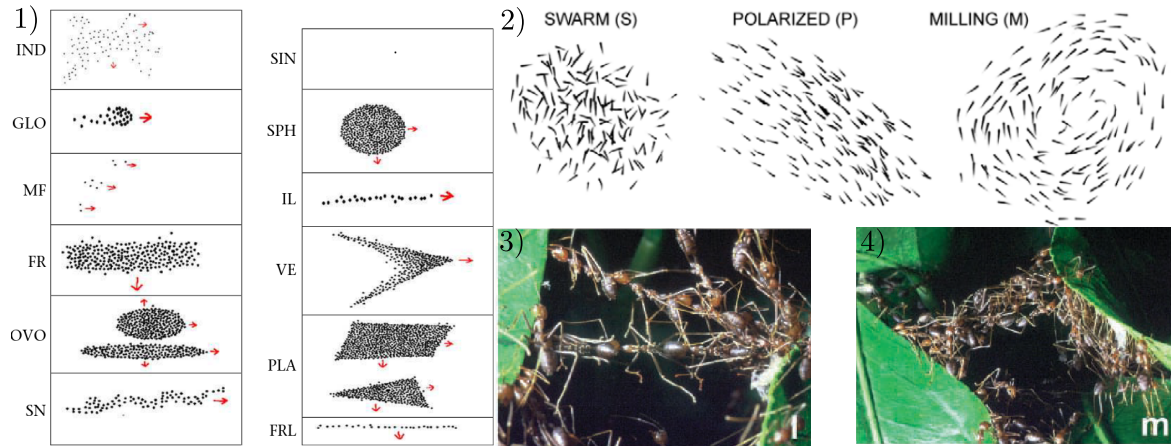


Figure 4.1: **Panel 1)** Example of different formation of birds deppending predation risk, obtained from [52]. **Panel 2)** Different formation of schooling fish, obtained from [57]. **Panel 3) - 4)** Aggregation of ants forming a bridge, obtained from [58].

Over time, further developments in the study of group dynamics have incorporated methods such as dynamical maximum entropy to predict the alignment of ordered groups [50]. Following a maximum entropy approach, network reshuffling was later studied [51]. These behaviors, however, can change due to external factors, such as predation risk, which influences the formation and density of flocks [52]. In addition, individual characteristics can also affect collective behavior [53].

There are also self-organized groups of smaller flying animals whose collective behavior is even more complex than that of larger species. For example, bees are capable of dividing labor as a result of social interactions among individuals [54]. Remaining within the field of insects but shifting to a solid medium, ants exhibit similar patterns of labor division. Their organization can transition between ordered and disordered states depending on colony size. The disordered state typically occurs when the number of foraging ants is small, due to the infrequent discovery of food [55]. However, even when the colony is large enough to sustain a greater number of foragers, problems can still arise. In particular, some ants may remain stationary, occupying tunnels and thereby reducing the overall flow rate [56].

Another characteristic that arises from self-organization in ants—one not possessed by all animals—is their ability to self-assemble to perform specific tasks. Examples include the formation of rafts, bridges, or columns, where each individual uses its legs or jaws to grasp another and remains in place until the collective goal is achieved. Naturally, certain factors influence these self-assemblages, one of the most significant being colony size [58]. Interestingly, these structures possess some viscoelastic properties, when a certain stress is applied, they tend to return to

their original place, resulting in an elastic behavior. At the same time they exhibit a viscous behavior when objects are able to sink in the aggregate, the same way they would do in a viscous fluid [59]. This opens the possibility for ants to be used as smart materials.

There are also animals that form groups while inhabiting more complex environments, such as water. Regardless of the medium, different species often display similar behaviors and dependencies. For example, the dynamics of schooling fish can be predicted, typically resulting in three main configurations, with variations depending on group size [57, 60, 61].

These are just few examples of large animal groups that, interestingly, share common characteristics of self-organization. This process begins at the level of the individual but emerges as a collective, temporary order through direct or indirect interactions among organisms, ultimately allowing them to achieve a common goal [62]. The study of macroscopic agents reveals that self-organization is not limited to large animal groups. At smaller scales, microscopic agents such as bacteria, colloidal particles, and artificial swimmers also exhibit analogous self-organized behaviors, although these are driven by different physical principles, including thermal noise and low-Reynolds-number hydrodynamics.

4.3 Microscopic Agents

As discussed in the previous section, the term active matter is not limited to microscopic systems but also applies to animal groups. However, the focus of this thesis will be on the former.

We have already defined how a passive brownian particle acts, therefore let us review the key difference of active and passive ones. Passive particles undergo mere diffusion motion, whereas active particles follows stochastic differential equations according to [63]:

$$\frac{d}{dt}x(t) = v \cos \varphi(t) + \sqrt{2D_T}W_x, \quad (4.1)$$

$$\frac{d}{dt}y(t) = v \sin \varphi(t) + \sqrt{2D_T}W_y, \quad (4.2)$$

this is known as the active brownian particle (ABP) model, which describes a particle that tries to move in a straight line, where W_x , and W_y represent their corresponding Wiener process, and v is the mean velocity. As stated before, in the limit

$$\lim_{v \rightarrow 0} v \cos \varphi(t) + \sqrt{2D_T}W_x, \quad (4.3)$$

the motion becomes purely diffusive, and the particle is characterized as passive brownian particle. In this limit, the dynamics reduce to the standard Brownian motion model, the simplest

representation of a particle undergoing thermal noise alone. Although active particles manifest persistent motion, they still display stochastic fluctuations; it is uncommon for them to move exactly in a straight line. This deviation often arises from chirality, which refers to geometric or dynamical asymmetry in the particle's structure or propulsion mechanism. There are three different forms of asymmetry: rotational, reflexional, and a combination of the two. A particle that is not superimposable to its mirror reflection, it is said to be chiral. Chirality is actually the name for a non-reflexive-symmetric particle, as exemplified by our hands, from which the actual word originates [64]. To account for the random reorientation of the propulsion direction, an additional stochastic term describing rotational diffusion is introduced:

$$\frac{d}{dt}\varphi = \sqrt{2D_R}W_\varphi, \quad (4.4)$$

where D_R is the rotational diffusion coefficient and W_φ represents a Wiener increment associated with the rotational angular noise.

In spite of the practicity of this model, there are other ones that better capture the dynamic of certain microorganisms. A notable example is the run and tumble particle (RTP) model, a type of motion that characterizes *E. Coli* bacteria. This displacement consists of quasi-linear "runs" for a random period of time to then randomly reorient itself ("tumbles"). The RTP model has been used to study the statistics local time of a particle in one dimension [65], as well as extensions two-dimensional analyses [66]. The describing equations is given by:

$$\frac{d}{dt}x = v\sigma(t), \quad (4.5)$$

where v is the speed of the particle and $\sigma(t)$ the particle's direction. To describe the dynamics of active particles under a potential that also is affected by thermal fluctuations the Active Ornstein-Uhlenbeck Particle (AOUP) model can be used:

$$\frac{d}{dt}r = v(t) - \gamma^{-1}\Delta U(r(t), t) + \sqrt{2D_T}\xi(t), \quad (4.6)$$

$$\frac{d}{dt}v = -\gamma_R v(t) + \sqrt{2D'_R}\eta(t), \quad (4.7)$$

where $\xi(t)$ and $\eta(t)$ follows the same principle as the thermal noise defined in Eq. (2.8) [67]. Showing there are different ways to study mathematically the movement of active brownian particles, these biological systems are autonomous and free to move and organize for survival [68]. Despite these limitations to control, researchers have been developing new methods to achieve self-propulsion that mimic natural processes. In the following subsections, we will introduce a few examples of different systems that have been created, as well as organic ones.

4.3.1 Artificial Systems

As discussed in Section 4.1, the definition encompasses various mechanisms of self-propulsion, and the list and discoveries are extensive.

Take, for example, PDMS platelets coated with Platinum by Ismagilov [69], which appears to be the first realization of this method. The motion itself is not performed by the particle, but by the layer of platinum (catalyst). This is a chemical reaction where the components move by the releasing of bubbles produced when a liquid (hydrogen peroxide) breaks down with the help of a catalyst. A catalyst is not affected by the reaction; therefore, the movement would occur indefinitely. In fact, under the experiment's conditions, they achieved an uninterrupted motion of approximately 2 hours. When observing the motion, they saw that they do not move in a straight line but rather in a circular manner, which is due to their chirality. They observed this behavior in all the particles; however, it was not completely identical due to thermal noise.

This experiment opened up the possibility of other setups; instead of the previous one, where flat plates were used, does this behavior depend on the shape of the particle? Paxton [70] did a similar experiment, utilizing rods with a diameter of 370 nm , with 2 stripes of platinum and gold, each one of $1\text{ }\mu\text{m}$ long in the direction of the long axis. While platinum is a catalyst for hydrogen peroxide; however, the twist here is that gold is not. Although the setup was similar, using the same chemicals, the results differed. They observed that the rods had a tendency to move along their elongated section, particularly in the direction pointing towards where the platinum was located, yielding a different result from the previous experiment, where the particle moved in the opposite direction to the platinum.

Not so much time later, Dreyfus [71] claimed that at that point, there was no artificial swimmer that had a *controlled swimming motion*. To remedy this, they combined organic and artificial elements; they used superparamagnetic filaments that respond to a magnetic field. These filaments are attached to a red blood cell, joining multiple cells to obtain a chain. To control the behavior of the filaments, they used two magnetic fields: a constant field parallel to the filament and a sinusoidal field perpendicular to the filament. With this approach, they were not only able to control the direction but also the speed by adjusting the frequency of the sinusoidal field, and the angle towards the parallel field.

However Howse [73] established the experimental basis for active Brownian particle dynamics by studying self-motile colloidal particles that use chemical reactions catalyzed on their surface to achieve autonomous propulsion. They demonstrated that at short times, these particles exhibit substantial directed motion with velocity dependent on fuel concentration, while at longer times, the motion transitions to a random walk with enhanced diffusion coefficients. This work provided a comprehensive experimental validation of the theoretical active Brownian particle

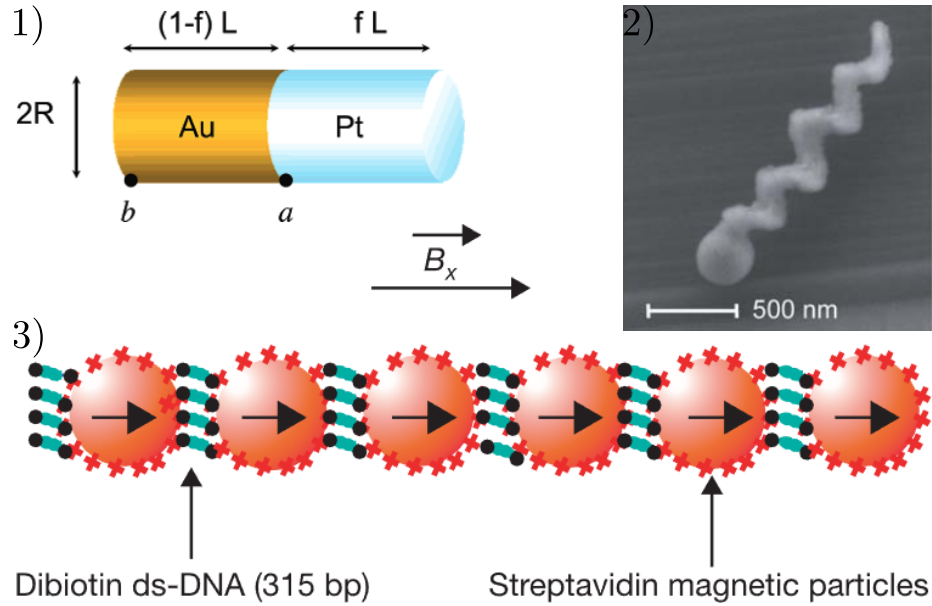


Figure 4.2: **Panel 1)** shows the configuration of nanorods of Gold (Au) and Platinum (Pt), obtained from [70]. **Panel 2)** Shows a Silicon Dioxide nan rod, obtained from [72].**Panel 3)** shows a chain of red blood cells linked with superparamagnetic filaments, obtained from [71].

model and established this model as the standard mathematical framework for describing such systems through stochastic differential equations [74]. The experiments were done by coating polystyrene shperes with a layer of platinum, creating Janus particles, similarly to the plates and the nanorods, which will be the responsible of the propulsion method; Nontheless, the tumble behavior is not inherently of the particle's shape, there have been assymetric artificial particles with an L shape that undergoes the same pattern [75].

Figure 4.3 helps visualize how the motion varies according to their velocity. When the average velocity is zero, the linear behavior of the MSD represents a diffusive behavior, whereas when it is different it is considered to be ballistic, and how good the model can predict and reproduce experiments.

Tierno [76] proposed a new mechanism where two linked paramagnetic colloidal particles of different sizes, need no deformation for propulsion. Their setup consists of colloids dispersed in water above a flat glass plate in the presence of a precessing magnetic field parallel to the plate. Here, the plate plays an important role for the propulsion, due to the dynamics when particles are near a boundary. When the smaller one is near the glass, the viscosity increases, resulting in lateral translation of the small colloid.

Looking at biomedical applications, Ghosh [72] proposed a system where helical screw nano

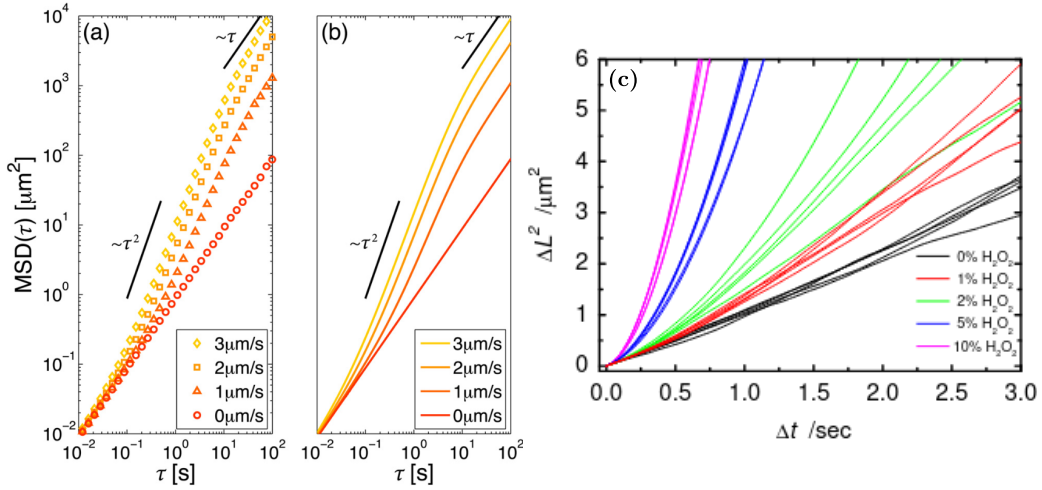


Figure 4.3: MSD for brownian particles with different velocites. **Panel a)** shows the result from simulations. **Panel b)** shows the theoretical calculation, obtained from [63]. **Panel c)** MSD for different velocities of polystyren spheres for different concentrations of Hydrogen Peroxide, obtained from [73].

propellers are driven by an homogenous magnetic field. Their control is so precise that it can be manipulated with a tolerance of microns. Their size is approximately 200-300 nm, making them ideal for navigating confined spaces and not being intrusive. Half of the helices are covered with cobalt, which has ferromagnetic properties, and then placed between two electromagnetic poles with a homogeneous precessing magnetic field, making the magnetic moment align with their long axis. Since the ferromagnetic part has a natural magnetic moment, it aligns with the external field, causing it to rotate along the helix. For each rotation, the particle moves either forward or backward, depending on the frequency of the helix's geometry and the direction of the magnetic field.

4.3.2 Natural Systems

We note how researchers have developed numerous strategies to achieve what was already accomplished by nature over a long period. In this section, we will present some examples of biological agents that inspired this thesis.

In a research by Corkidi [77] spermatozoa behavior was studied in a 3-dimensions space mimicking their real environment in searh for eggs, what they found was a helical trajectory, shown in Figure 4.4, being a pretty similar response, and obtaining a non-space dependant behavior.

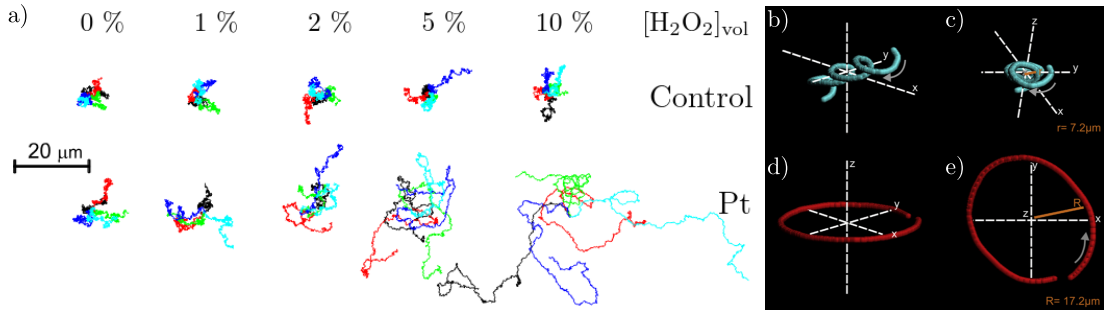


Figure 4.4: Trajectories of polystyrene platinum coated spherical particles for different peroxide concentrations, upper row show a control bead and the lower a platinum bead, obtained from [73]. Trajectory of the spermatozoa for **a**, **c** free space, and **b**, **d** confined 2-dimension space. Obtained from [77].

It seems we cannot avoid randomness even for active particles and obtain a more controllable movement for specific tasks. In a regime where viscous forces are predominant, any small fluctuation breaks the symmetry and the direction of the particle. Nature, as always, has evolved elegant solutions to this challenge through various biological mechanisms. A prime example is E. Coli, which employs helical flagella that can rotate both clockwise and counterclockwise, generating two distinct types of motion that researchers have termed "run"—swimming in a straight line—and "tumble"—rotation in a random direction. This behavior also depends on the medium's viscosity and random fluctuations [78]. The way E. Coli achieves a "run" state is due to their flagella which has two different motions for its power and recovery strokes, simulating those of a human's breast strokes, it is a great opportunity to harness the directed motion of the particle and see if it is possible to obtain work of it.

Marine bacteria are another example of an organic microswimmer, which can obtain individual speeds ten times faster than that of E. Coli ($40 \mu\text{ms}^{-1}$) [79, 80]. Marine bacteria have a similar swimming mechanism as E. Coli, responding to amino acids, and utilising a run and reverse motion, different from the run and tumble, allowing them to stop and reverse their direction, making it more efficient [81]. A study by Barbara [82] aimed to investigate how they swim to obtain its nutrients. Interestingly, thanks to the reverse motion system, marine bacteria were able to turn multiple times in the direction of the nutrients, thereby tracking them with fewer attempts. Another remarkable example of biologically active matter is the green algae *Chlamydomonas reinhardtii*. This unicellular microorganism swims using two anterior flagella that beat in a breaststroke-like motion, propelling the cell forward through the water. Unlike bacteria, which rotate their helical flagella, *C. Reinhardtii* relies on the coordinated motion of paired flagella, leading to straight swimming when both are synchronized and to turning when

the coordination is lost [83]. Because of this, *Chlamydomonas* is often used as a model organism to understand how eukaryotic cells achieve motility at low Reynolds number.

Another type of biological microswimmer is found in protozoa such as *Paramecium*. These ciliates are covered with thousands of cilia that beat in a coordinated manner, producing smooth gliding motion through viscous fluids [84]. Cilia not only enable propulsion but also allow *Paramecium* to sense and respond to chemical gradients in their environment, demonstrating an early form of mechanosensory feedback in microswimmers.

Sometimes, bacteria organize themselves in a way the density is high enough that they behave like a *Liquid Crystal*. This phenomenon usually appears in systems of elongated bacteria, where their shape and mutual interactions make the whole sample behave as something between a solid and a liquid, observing local ordering, due to some of its degrees of freedom are ordered while some other are not. This intermediate state is what gives rise to the name *liquid crystal*. These systems show characteristic features such as local orientation—resulting from the elongated shape of the cells, which allows this property to be measured—and the presence of topological defects, among others [85]. There has been attempts to create artificial liquid crystals that mimic the biological ones like the one by Sokolov [86] where with disodium cromoglycate, controlled by an acoustic field. Immune system cells, such as neutrophils, also display active motility, although they crawl rather than swim. Neutrophils move by extending actin-rich protrusions (lamellipodia) and contracting their cell body, enabling them to pursue pathogens in tissues [87]. While their propulsion mechanism differs from that of flagellated or ciliated organisms, neutrophils still exemplify how living systems consume energy internally to generate directed motion.

These diverse biological strategies demonstrate how nature has evolved multiple solutions to achieve motion in environments dominated by viscous forces. Each of these mechanisms—flagellar beating in algae, ciliary coordination in protozoa, or actin-driven crawling in immune cells—highlights the central role of active matter principles in biology. But, is their locomotion enough to produce work?

4.4 Obtaining Work from Active Matter

A fundamental question in active matter research is whether the continuous energy consumption and motion of biological microswimmers can be harnessed to perform useful work. In nature, molecular motors such as kinesin, dynein, and myosin already accomplish this inside cells, driving processes like vesicle transport, muscle contraction, and chromosome segregation. Inspired by these nanoscale examples, researchers have investigated whether intact organisms at the mi-

croscale can be used as biological engines outside their natural environments [88].

One particularly illustrative example comes from the work of Weibel [89], who introduced the concept of “*microoxen*” — motile cells of the green alga *Chlamydomonas reinhardtii*. In their study, the authors exploited the flagellar beating of *Chlamydomonas* to transport microscale loads such as polystyrene beads. By chemically attaching the beads to the cell wall, these algae were able to carry particles 1–6 μm in diameter without significantly reducing their swimming velocity (100–200 $\mu\text{m/s}$, similar to unmodified cells).

An important feature of this work was the ability to control and manipulate the cells. Because *Chlamydomonas* exhibits positive and negative phototaxis [90], its direction of motion could be guided in microfluidic channels by alternating visible light sources. This allowed them to steer cargo-carrying cells back and forth repeatedly over distances of up to 20 cm. Moreover, by including a *photocleavable chemical linker* between the load and the cell surface, they enabled the controlled release of particles using UV light, allowing cells to pick up, transport, and drop off cargo on demand. This study served as inspiration for using living active matter to perform mechanical work. On one hand, it demonstrates that whole microorganisms can act as microscopic carriers, and self-sustaining energy supply. On the other hand, it also underscores practical limitations: maintaining living cells, and preventing adhesion to surfaces.

Qin [91] attempted to harness the dynamics of the decomposition of previously studied hydrogen peroxide, but rather than creating a system of linear motion, they employed it in a different manner. It is a similar approach as the nanorods, that use stripes of Pt and Au, this time they use a small surface, resembling a patch in one part of the rod, this configuration makes the release of oxygen bubbles in a lateral being capable of producing torque on the rod and therefore making it spin, thanks to this, they were able to create a nanorotor. However, we can argue that they are not harnessing the behavior of active matter to create work on an external object, but rather active matter does work by moving itself.

Another novel demonstration of obtaining work from active matter was presented by Hiratsuka [93], who developed a microrotary motor powered by the gliding bacterium *Mycoplasma mobile*. Unlike flagellated swimmers *E. coli* or *Chlamydomonas*, *M. mobile* moves by gliding over solid surfaces at speeds of 2–5 $\mu\text{m/s}$, using sialic proteins in the surface of the track. The authors harnessed this motility by integrating living cells into lithographically fabricated microdevices. Their microrotary motor consisted of a circular silicon track, into which *M. mobile* cells were introduced asymmetrically so that the majority moved in a unidirectional loop. A 20 μm silicon dioxide rotor with protrusions that fit into the circular track was then docked, and cells were chemically linked to its surface via biotin–streptavidin interactions. As the bacteria glided along the track, they pulled the rotor, producing unidirectional rotation at rates of 1.5–2.6

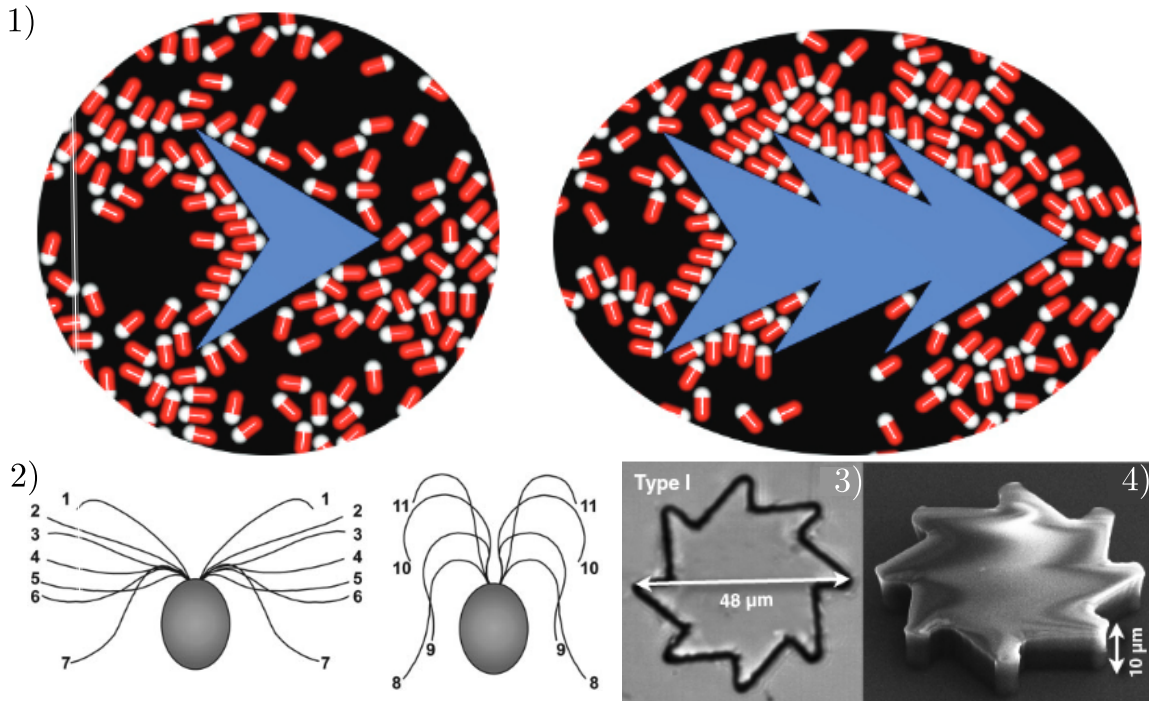


Figure 4.5: Experiments that harness bacteria motility. **Panel 1)** shows how the bacteria accumulates in the concave sections of the shuttle, finally aligning parallelly, obtained from [92]. **Panel 2** drawing of Chlamydomonas Reinhardtii's movement, obtained from [89]. **Panel 3) - 4)** shows an example of ratchet used in experiments, made by lithography, obtained from [15].

revolutions per minute (rpm). The torque generated by individual cells was estimated to be $2\text{--}5 \times 10^{-16}$ N·m, sufficient to overcome viscous drag at the microscale. This work represents a successful integration of living motile cells with inorganic micromachinery, demonstrating that whole microorganisms can be harnessed to drive artificial devices.

Angelani [92] noticed how asymmetric geometry can be used to harness the randomness of particles to obtain work from them. Using numerical simulations, they mimicked elongated motile bacteria, and the object to move consisted of an arrow-shaped structure with a varying number of teeth, ranging from 2 to 8. They saw that some particles get trapped between the spaces of the teeth, aligning themselves, making it possible to push the *shuttle*, and due to dynamics, they eventually get unstuck and return to swim free in the solution. The simulations were performed in 2 dimensions, where bacteria were able to push the object.

Beyond the use of single microorganisms as engines, researchers have also looked at how collective active matter might be used to produce work. Thampi [94] showed in simulations

that dense active fluids—like bacterial suspensions or mixtures of microtubules with motor proteins—can display mesoscale turbulence that can be rectified to move micromachines. In their setup, a square array of symmetric microrotors was placed inside an active nematic fluid. Although the rotors were geometrically identical, the system broke symmetry on its own: neighboring discs settled into an alternating spin pattern, rotating in opposite directions. In this way, disordered turbulent flows were turned into a regular and steady source of rotation. The extent and stability of the rotation depended on rotor size and spacing, with the best results when the separation was comparable to the natural vortex size of the active turbulence. This study is useful here for two reasons. First, it shows that work can be obtained from active turbulence without introducing asymmetry or applying external fields. Second, it illustrates how geometry and confinement help stabilize active flows—ideas that will be relevant again in this thesis when we study colloids and ratchet systems under external driving.

A central question in active matter is how to harness the continuous energy consumption of self-propelled agents to perform useful work. Inside cells, proteins such as kinesin and dynein already fulfill this role at the nanoscale, but the prospect of exploiting entire microorganisms as microscopic engines is especially appealing. Early studies demonstrated that bacteria could be attached to synthetic objects and used to propel them forward [89, 93]. The resulting motion, however, was generally random.

A major advance came with the work of Di Leonardo [15], which served as inspiration for this thesis, showing that geometry alone can guide bacterial motion without the need for external fields. In their experiments, sawtooth-shaped microgears with diameters of approximately 48 μm were immersed in dense suspensions of motile *E. coli*. The bacteria accumulated and aligned at the concave corners of the gears, collectively exerting a torque that rotated the structures. At cell concentrations on the order of 10^{10} mL^{-1} , the gears achieved steady angular velocities of about 2 rpm. This behavior follows the mechanism described by Angelani et al. (2010), where cells become transiently trapped between the asymmetric teeth, pushing against the walls and generating directed motion [92]. Interestingly, the authors also tested different geometries. As expected, asymmetric rotors produced net rotation, while symmetric ones yielded zero average angular velocity, underscoring the importance of symmetry breaking in rectifying bacterial motion.

This result demonstrates that combining bacterial activity with asymmetric boundaries can act as a ratchet, transforming random fluctuations into directed motion. The concept recalls the Feynman ratchet thought experiment, but here it is realized in a living system, powered solely by bacterial metabolism. Such bacterial ratchets not only provide fundamental insight into nonequilibrium statistical mechanics but also suggest potential applications in microfluidics, where pumps and mixers could operate autonomously without external energy inputs.

Chapter 5

Magnetically Driven Colloidal Systems

We can see that biological active matter is effective at transporting or moving objects. The drawback, however, is that these systems always require a constant supply of energy. So far, there is no unlimited energy source available for this purpose. An exception are thermophoretic particles, which only need a beam of light to create a temperature gradient. In fact, some experiments have combined this principle with machine learning models, allowing particles to be guided toward a target region while reducing the impact of thermal noise [95]. The limitation, though, is that only a relatively small number of particles can be manipulated in this way, which is not enough to drive something like a rotor. Magnetism has long been a subject of interest because of its wide range of applications, from medical imaging and targeted drug delivery [96–98] to lab-on-a-chip technologies [99]. More recently, it has also been used to control and organize colloidal systems. For example, Massana-Cid [100] showed that paramagnetic colloidal particles exposed to oscillating magnetic fields can self-assemble into large-scale “colloidal carpets”, as shown in Figure 5.1, that can move and even repair themselves. These carpets form because of the combined effects of magnetic dipole–dipole interactions and hydrodynamic coupling, and their degree of order can be tuned by changing the parameters of the external field.

This thesis focuses on paramagnetic colloids. Their key property is that the magnetic dipoles align with an external field, but once the field is removed, the dipoles lose their orientation and the material no longer shows magnetic order. The origin of this effect lies in the electronic and spin configuration of the atoms. A simple example is molecular oxygen, O_2 , which has two unpaired valence electrons with the same spin. This imbalance leads to a net magnetic moment, giving rise to paramagnetism. The underlying principle is explained by Hund’s rule.

By themselves, paramagnetic particles cannot be considered active matter, even in the presence of a magnetic field. Several experiments have tried to induce motion in these systems, and one promising route is through Brownian rectification. For example, Tierno [18] studied para-

magnetic colloids placed above a ferrite garnet film, shown in Figure 5.1. The film contained permanent magnetic domains aligned along the x -axis, with alternating directions, while the colloids were subjected to a circularly precessing magnetic field in the y – z plane.

With these parameters, and by varying only the driving frequency, four regimes of motion were identified. At the highest frequencies, the particles entered a pinned state, meaning the colloids did not translate. Tierno also tested elliptic magnetic fields and observed that, depending on the field magnitude, the particles displayed either attractive or repulsive interactions. These behaviors arise from the dipole–dipole potential between particles, given by

$$U_{dd} = \frac{\mu}{4\pi} \left(\frac{m_i m_j}{r_{ij}^3} - \frac{3(m_i \cdot r_{ij})(m_j \cdot r_{ij})}{r_{ij}^5} \right), \quad (5.1)$$

where m_i and m_j are the magnetic moments of particles i and j , and r_{ij} is their separation vector.

A subsequent study by Straube and Tierno [101] provided a deeper understanding of these dynamics by analyzing the role of synchronization and thermal noise. Using the same ferrite garnet film with periodic magnetic domains, they investigated the motion of a single paramagnetic colloid driven by a rotating magnetic field. At low driving frequencies, the particle remained synchronized with the moving magnetic potential, resulting in constant-speed transport at the same velocity as the traveling landscape. Above a critical frequency, however, the particle lost synchronization, entering an asynchronous regime characterized by intermittent sliding and a reduced average speed.

To describe these results, Straube and Tierno proposed a simplified analytical model based on the overdamped Langevin equation, which accounted for both deterministic forces and thermal fluctuations. Importantly, their model showed excellent agreement with experiments and revealed how thermal noise smooths the sharp transition between synchronous and asynchronous regimes. This highlights the interplay between deterministic driving and stochastic forces in rectification phenomena, and demonstrates how even passive colloids can be controlled and transported through external fields when symmetry is broken.

A year later, they used the same system with a rotating magnetic field whose ellipticity could be tuned [19]. The effect of this field was to create an asymmetric traveling potential that rectified Brownian motion and transported the particles across the surface. One of the main results was that the interaction between particles could switch from repulsive to attractive just by adjusting the ellipticity of the field. In the attractive case, particles came together into stable doublets that moved with constant velocity along the magnetic stripes. They measured the dipolar forces that caused this binding and proposed a model that matched well with the experiments. This shows that not only single-particle motion can be controlled, but also collective effects like chain for-

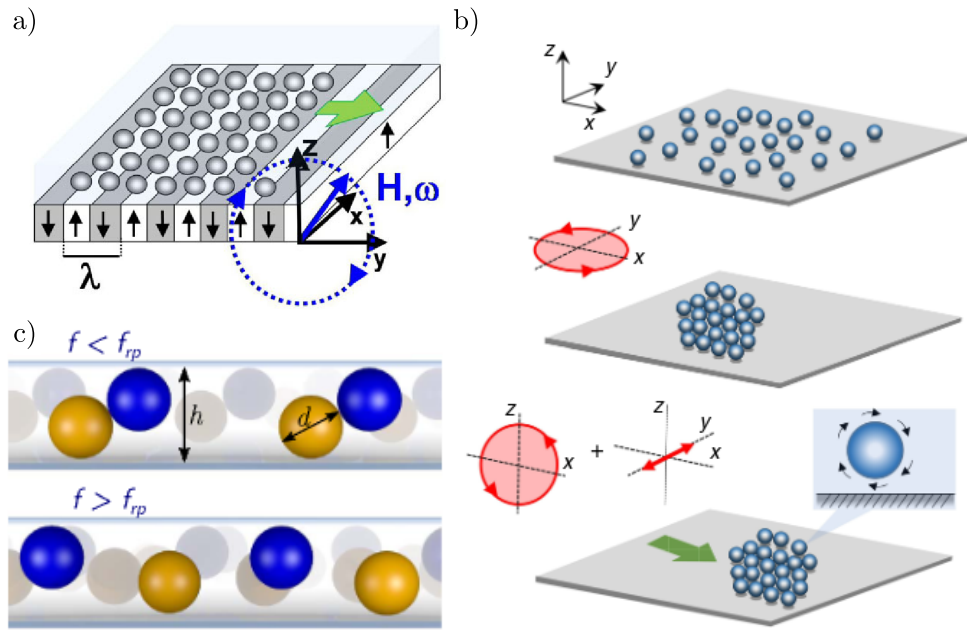


Figure 5.1: **Panel a)** shows the system with garnet films used to obtain net motion. The green arrow depicts the direction of the colloids, and the blue arrows show the magnetic field, obtained from [18]. **Panel b)** show the process of how the colloids form a crystalline carpets and the direction of the film, depicted with the green arrow, due to the rotation of the rolling colloids, obtained from [100]. **Panel c)** shows spherical colloids in a confined space with different external field frequencies, obtained from [20].

mation and cooperative transport. The fact that this can be tuned with an external field suggests possible uses in microfluidics or lab-on-chip devices, where clustering or separation of particles can be useful for transport, mixing, or sorting.

More recently, Stoop [102] studied a dense monolayer of paramagnetic colloids driven above a triangular lattice of magnetic bubbles using a rotating magnetic field. The external field generated a two-dimensional traveling wave ratchet that transported the particles across the substrate. While single colloids showed no preferred direction of motion, collective interactions at higher densities led to a spontaneous symmetry breaking. In this regime, the particle current locked along one of the crystallographic axes of the lattice, producing a transversal current even though the driving direction was set between two symmetry axes. They also reported that this locking could be polarized by adding a weak bias field, which made one direction energetically favorable over the other. At intermediate densities, elongated clusters of particles formed and moved coherently, showing that dipolar interactions stabilize directional locking. At very high densities, however, the effect was lost as the colloids formed a percolating network covering the entire substrate. This work highlights how collective effects can generate robust directional transport that does not appear at the single-particle level. It shows that by controlling density and external fields, transport in colloidal systems can be tuned or polarized, which is useful for applications such as particle sorting and microfluidic control.

An interesting study by Massana-Cid [20] analyzed the behavior of paramagnetic particles coated with nanoscale iron oxide grains confined within a space of suitable height, depicted in Figure 5.1, to prevent column formation while still allowing vertical (z-axis) motion. Under a static magnetic field, the particles tended to organize into triangular or square lattices [103], and in some cases formed labyrinth-like structures. To avoid this ordering, the authors applied a conical time-dependent precessing magnetic field rotating around the z-axis. They found that the frequency of this field played a key role in the dynamics of the system: at certain frequencies, the particles exhibited collective rotation. However, because of the dense packing, strong interactions between neighboring particles significantly affected their motion.

The work of Ostinato [21] can be seen as a continuation of the study by Massana-Cid, exploring the same type of confined paramagnetic colloids under precessing magnetic fields. While the first focused on the onset of collective rotation and structural organization, the latter extended the analysis to transport regimes and diffusion properties using equally both experiments and simulations. Under a spatially isotropic field, the particles did not exhibit any net current but showed a strong increase in diffusion—up to sixty times higher than that of undriven colloids. This enhanced diffusion resulted from a continuous position exchange between particles near opposite walls, resembling a “ceilidh dance” [104] of dimers that periodically bind and unbind.

In contrast, introducing a small spatial anisotropy by tilting the precession axis ($\delta \neq 0$) generated a robust bidirectional current. In this regime, colloids organized into two parallel flows moving in opposite directions, achieved by synchronized particle exchanges across the two planes. The magnitude of this current was highly tunable by varying both the driving frequency and the tilt angle, reaching maximal values when particles jumped exactly one lattice constant per field cycle. Remarkably, this bidirectional transport was robust against single-particle defects but could be disrupted by the introduction of “magnetic holes” (nonmagnetic inclusions in the ferrofluid), which acted as localized defects that broke the current pathways.

These results provide a powerful demonstration of how geometrical confinement and external field anisotropy can convert random thermal motion into ordered transport, without the need for field gradients. They highlight new opportunities for designing microfluidic devices where colloids could be directed, mixed, or sorted by simply tuning the parameters of an external homogeneous field.

Part III

Methods

Chapter 6

Simulations

6.1 Paramagnetic Colloids Dynamics

The system studied in this thesis consists of an ensemble of paramagnetic colloidal particles confined in a quasi-two-dimensional geometry and subjected to an externally applied precessing conical magnetic field. Each colloid is a spherical particle of radius r_{mag} suspended in a Newtonian fluid of dynamic viscosity η . The suspension is bound by two parallel glass plates separated by a distance h , such that $h \lesssim 2R$. This strong confinement restricts particle motion primarily to two dimensions, while still allowing limited vertical displacement.

Numerical simulations provide a powerful framework to reproduce and analyze physical phenomena under controlled conditions. Unlike experiments, they allow for precise manipulation of initial parameters, systematic testing of hypotheses, and straightforward replication of results. In particular, simulations are invaluable when dealing with microscopic systems, where stochastic effects and complex interactions can make experimental observations challenging.

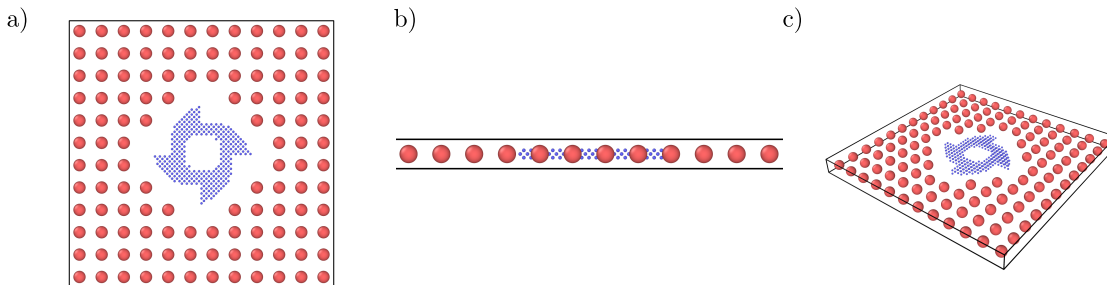


Figure 6.1: System overview for a 4 spikes spin up ratchet at time 0. Panel a) shows the top view. Panel b) shows a lateral view. Panel c) shows a perspective view.

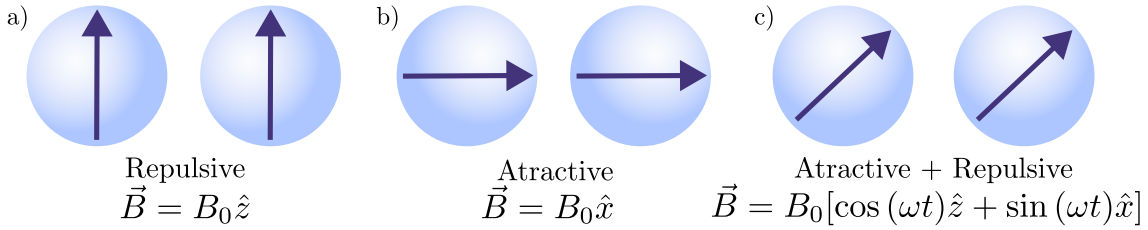


Figure 6.2: Interaction between a pair of paramagnetic colloids when a) a constant field in \hat{z} is applied, b) constant field in \hat{x} is applied, and c) when a rotating field is applied in the plane \hat{x}, \hat{z} .

Let us first describe the ensemble of paramagnetic colloids. The particles are modeled after Dynabeads M-280 Streptavidin, which possess paramagnetic properties: they acquire a magnetic moment only when an external magnetic field is applied. Once the field is removed, the particles exhibit no remanent magnetization, unlike ferromagnetic materials. The induced magnetic moment aligns instantaneously with the direction of the applied field. When considering the simplified case of two interacting particles, the dipole–dipole interaction can be either attractive or repulsive depending on their relative orientation, as illustrated in Figure 6.2. If the external magnetic field is slowly rotated, the dipoles follow its motion, and the interaction angle between the particles continuously varies from attractive to repulsive, however the average interaction over time is attractive [100]. There exists, however, a particular angle at which the interaction energy vanishes, it is neither attractive nor repulsive. This critical value is known as the magic angle [105, 106], given by

$$\theta = \arccos \frac{1}{\sqrt{3}} \approx 54.7^\circ.$$

When a pair of particles is placed inside a confined space under a constant magnetic field designed to induce repulsive interactions, the particles will displace from each other until reaching equilibrium. However, when considering the collective dynamics of an infinite chain of particles, where individual displacement is restricted by the presence of neighboring particles, the system instead exhibits vertical motion, as illustrated in Figure 6.3. By varying parameters such as particle packing density and the height of the slit pore [103], distinct structural patterns can emerge in the equilibrium configurations. Nonetheless, when the confinement height exceeds a critical threshold, the particles tend to form dimers due to reduced repulsive constraints and enhanced dipolar coupling.

Considering the same confined space under the presence of a conical external magnetic field, the dynamics of the colloids vary with the driving frequency. At low frequencies, the particles form pairs (dimers) that rotate synchronously with the magnetic field; this regime is referred to

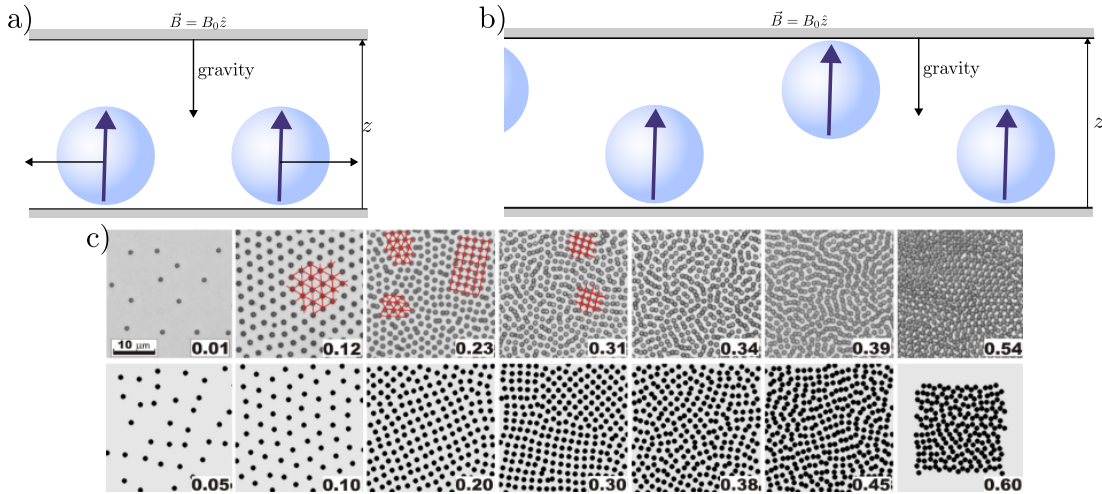


Figure 6.3: Dynamics of paramagnetic colloids in confined space in the presence of gravity and a constant field applied in \hat{z} for a) a pair, b) an infinite chain. Panel c) shows the behavior of particles at 12.5 mT at different packings, bottom row shows experimental results, bottom row show simulations results, obtained from [103].

as the synchronous state. At high frequencies, the magnetic torque generated by the dipole interaction becomes smaller than the viscous torque, resulting in a rotational lag. In this regime, the dimers rotate asynchronously, meaning they still spin but no longer match the field's frequency. At even higher frequencies, another phase coexists—known as the rupture state—where the colloids cease forming dimers and instead arrange into a crystalline structure.

At intermediate frequencies, a transition state emerges in which the colloids exhibit both synchronous and asynchronous behavior. In this regime, particles periodically rotate, separate, and reattach to different neighbors; this state is referred to as the exchange or neighbor-exchange phase in this thesis. These states depend on several factors, including particle packing density and slit-pore height. Figure 6.4 illustrates some of these transitions for constant height and packing while varying the driving frequency. The neighbor-exchange state, in particular, displays random, ballistic-like trajectories that contribute significantly to the collective dynamics of the solid ratchet.

6.2 Molecular Dynamics

In this thesis, numerical simulations are employed to study the dynamics of colloidal systems at the microscale. Such systems are often dominated by thermal fluctuations and many-body inter-

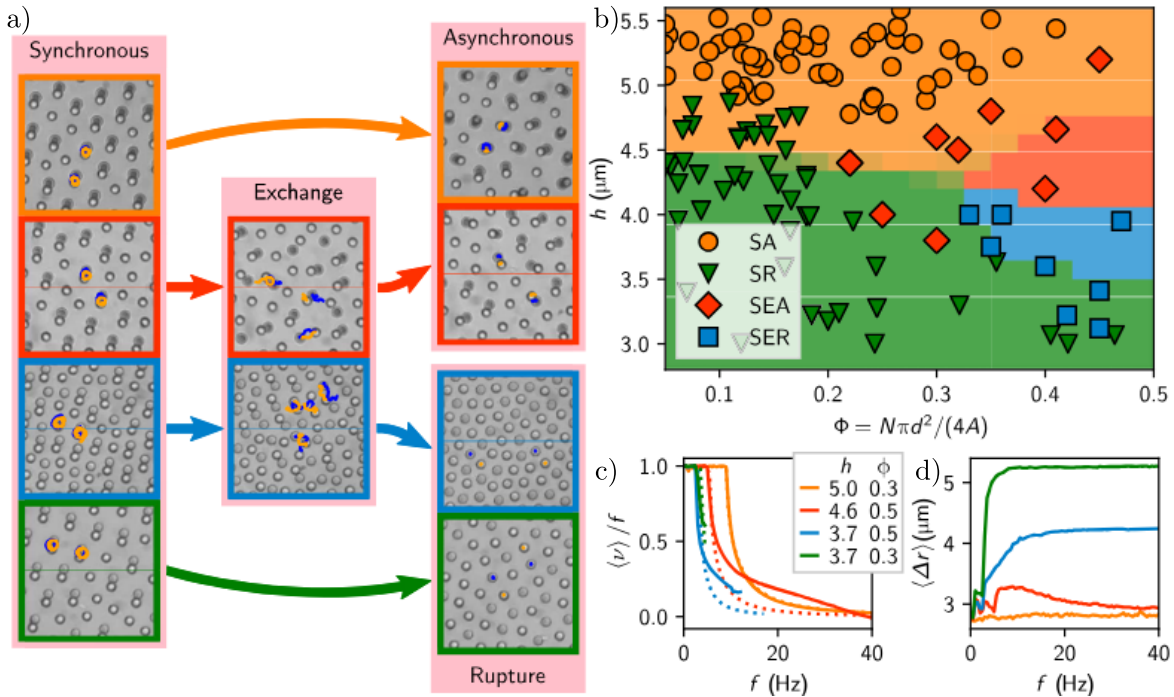


Figure 6.4: Panel a) shows the different phases observed when varying the external magnetic field. The synchronous phase corresponds to particles rotating in phase with the field. In the exchange phase, synchronization with the external field is lost, but particles continue to interact with their neighbors, exchanging positions. The asynchronous phase refers to particles that can no longer follow the external field and instead form dimers. Finally, the rupture phase occurs when particles fail to follow the rotating field but self-organize into a crystalline structure, panel b) shows the location of transition paths depending on packing and slit pore height. Panel c) shows relative dimer rotation respect to frequency. Panel d) shows the average particle separation respecto to frequency. Obtained from [20].

actions, making them difficult to probe experimentally without advanced imaging and data analysis techniques. The primary computational approach used here is *molecular dynamics* (MD), which will be described in detail in the following sections. MD enables the integration of particle trajectories under the influence of deterministic and stochastic forces, providing direct access to observables such as mean-squared displacements, velocity correlations, and transport coefficients.

This thesis explores the physics of the system by using molecular dynamics, where randomness enters through thermal noise. As we saw in 2.2.1, the interactions can be derived from classical mechanics. In this case, Newton's second law gives the starting point to calculate the forces acting on a single particle. In other words, at each iteration of the simulation we need to evaluate the forces that each particle experiences. Taking equation (2.4) as a starting point, and adding labels for the different interactions, we obtain:

$$m\ddot{\vec{x}} = F_i^{\text{collision}} + F_i^{\text{drag}} + \eta(t), \quad (6.1)$$

where m_i is the mass of particle i , \vec{x}_i its position, and F_i^{drag} is the viscous force, written as $-\gamma\dot{\vec{x}}_i$, with γ the drag coefficient of the fluid. Since we are working at a scale where inertial effects are negligible, the term $m_i\ddot{\vec{x}}_i$ can be dropped. The random force $\eta(t)$ represents collisions with the solvent particles. In this thesis, η is taken as a Gaussian random force with $\langle\eta\rangle = 0$ and correlation $\langle\eta_i(t)\eta_j(t')\rangle = 2k_B T \gamma \delta_{i,j} \delta(t - t')$. This form will be used for non-paramagnetic particles.

For paramagnetic particles, we need to add the contribution of dipole–dipole interactions, which gives the modified equation:

$$0 = F_i^{\text{collision}} + F_i^{\text{drag}} + F_i^{\text{dd}} + \eta(t), \quad (6.2)$$

where F_i^{dd} according to [107] is described as force exerted for the dipole moment \vec{m}_i on a dipole \vec{m}_j :

$$\begin{aligned} \vec{F}_i^{\text{dd}} = & \frac{3\mu_0}{4\pi r^4} \left[(\hat{x}_{i,j} \times \vec{m}_i) \times \vec{m}_j + (\hat{x}_{i,j} \times \vec{m}_j) \times \vec{m}_i \right. \\ & \left. - 2\hat{x}_{i,j}(\vec{m}_i \cdot \vec{m}_j) + 5\hat{x}_{i,j}((\hat{x}_{i,j} \times \vec{m}_i) \cdot (\hat{x}_{i,j} \times \vec{m}_j)) \right], \end{aligned} \quad (6.3)$$

where $\hat{x}_{i,j}$ is the unitary vector of distance between dipoles. Since all magnetic dipoles are identical and aligned with the external magnetic field \vec{B}_{ext} , we can express the dipole moment as $\vec{m} = \chi V \vec{H}_{\text{ext}} = \frac{\chi V}{\mu_0} \vec{B}_{\text{ext}}$, where χ is the magnetic susceptibility and V is the particle volume. Substituting $\vec{m}_i = \vec{m}_j = \vec{m}$ and expressing in terms of the external field gives:

$$\vec{F}_{i,j}^{\text{dd}} = \frac{3\mu_0 m^2}{4\pi r^4} \left[2(\hat{x}_{i,j} \times \hat{B}) \times \hat{B} - 2\hat{x}_{i,j} + 5\hat{x}_{i,j}|\hat{x}_{i,j} \times \hat{B}|^2 \right], \quad (6.4)$$

where $m = \frac{\chi V B_{\text{ext}}}{\mu_0}$, $\hat{B} = \vec{B}_{\text{ext}}/B_{\text{ext}}$ is the unit vector along the external field, and $B_{\text{ext}} = |\vec{B}_{\text{ext}}|$.

This is the force applied by one particle, to obtain the total dipole interaction with all particles of the system, we should add them up, pair by pair:

$$F_i^{dd} = \sum_{i \neq j}^n F_{i,j}^{dd}. \quad (6.5)$$

We need to define the external magnetic field, which is a precessing field that forms a conical rotation of the form

$$\vec{B} = B_0[\cos \theta \hat{z} + \sin \theta \cos(\omega t) \hat{x} + \sin(\omega t) \hat{y}], \quad (6.6)$$

where B_0 is the amplitude and f the frequency of rotation of the magnetic field. The frequency plays an important role in the system dynamics. Depending on how fast the field rotates, it determines whether the internal magnetic dipole of each particle can follow it or not. At low frequencies, the dipoles rotate synchronously with the field, resulting in purely attractive or repulsive interactions. At higher frequencies, however, the dipoles cannot keep up, leading to a phase delay. In this regime, particles can exchange neighbors as the field continues to rotate.

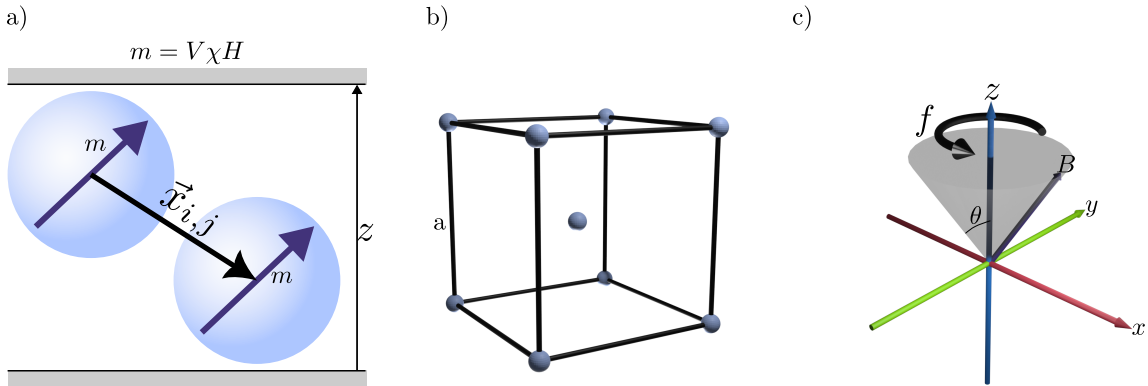


Figure 6.5: Panel a) Shows two paramagnetic particles with a distance $\vec{x}_{i,j}$ with the same dipole moment in a confined space in the z axis. Panel b) Shows a representation of a unitary body-centered cubic lattice used in the construction of the ratchet. Panel c) Shows the precessing external magnetic field used in the simulation.

To model contacts, we use a Weeks-Chandler-Andersen potential (WCA), which is a LJ with only a repulsive part [108]:

$$U_{i,j}^{WCA} = \begin{cases} 4\epsilon \left[\left(\frac{\sigma}{r_{i,j}} \right)^{12} - \left(\frac{\sigma}{r_{i,j}} \right)^6 \right] + \epsilon & r_{i,j} \leq r_c \\ 0 & r_{i,j} \geq r_c \end{cases} \quad (6.7)$$

where σ is the van der Waals radius, it is the point where the energy between the two particles is zero, ϵ is the well depth, since WCA does not have an attraction interaction, a correction factor of ϵ is added, and $r_c = 2^{1/6}\sigma$. This however, gives us the energy between particles, and we need the force, then we apply:

$$F = -\nabla U, \quad (6.8)$$

getting then

$$F_{i,j}^{WCA} = \begin{cases} 48\epsilon \left[\left(\frac{\sigma}{r_{i,j}} \right)^{12} - \frac{1}{2} \left(\frac{\sigma}{r_{i,j}} \right)^6 \right] \left[\frac{1}{r_{i,j}} \right] & r_{i,j} \leq r_c \\ 0 & r_{i,j} \geq r_c \end{cases}. \quad (6.9)$$

and adding all the interaction expected by each particle, we obtain:

$$F_i^{collision} = \sum_{i \neq j}^n F_{i,j}^{WCA}. \quad (6.10)$$

We want to see how the positions of the particles evolve over time with certain initial conditions, and to solve Eq. (6.2) this is why we need an integration method.

6.3 Euler-Maruyama Integration Method

The Euler-Maruyama is a numerical method used for stochastic differential equations which helps solve systems with Brownian motion [109, 110].

The overdamped Langevin equation for a particle reads

$$\dot{x}(t) = \frac{1}{\gamma} F(x, t) + \sqrt{2D} \eta(t),$$

where γ is the dynamic viscous drag, $D = k_B T / \gamma$ the diffusion coefficient, and $\eta(t)$ is normalized Gaussian white noise: $\langle \eta_i(t) \rangle = 0$, $\langle \eta_i(t) \eta_j(t') \rangle = \delta_{ij} \delta(t - t')$. Discretizing with timestep Δt and Wiener increments $\Delta W \sim \mathcal{N}(0, 1)$, the Euler–Maruyama update is

$$x_{n+1} = x_n + \mu F(x_n, t_n) \Delta t + \sqrt{2D \Delta t} \Delta W_n. \quad (6.11)$$

6.4 Definition of the Solid Ratchet

To create the solid ratchet we used basis vectors (or lattice vectors) which are the fundamental building blocks used to generate the entire crystal lattice by translation. These vectors define the geometry of the unit cell, and by repeating the unit cell across space, we can form the overall lattice structure. Here, a body-centered cubic (BCC) lattice was chosen since the stability which proved to be stable under thermal fluctuations. The conventional unit cell for a BCC lattice is a cube with a lattice point at each corner and one at the body center. The vectors defining this cube are simple, orthogonal, and given by:

$$\vec{R} = m(a\hat{x}) + n(a\hat{y}) + p(a\hat{z}) + \delta \frac{a}{2}(\hat{x} + \hat{y} + \hat{z}); \quad m, n, p \in \mathbb{Z}, \quad (6.12)$$

where a is the lattice constant (the side length of the cube), and δ is either 0 or 1, depending if we are referring to the centered particle. Once defined the basis vectors, with help of a script we enter the required parameters that will define the size of the solid ratchet that is defined by a modulated radius function that creates N teeth around the azimuthal direction. The angular coordinate $\phi \in [0, 2\pi)$ is traced in the Cartesian coordinates (x, y) .

$$R(\phi) = R_0 + A \cdot S\left(\frac{f\phi}{2\pi}\right) - \frac{A}{2} \quad (6.13)$$

where $S(x)$ is the sawtooth function, A is the amplitude of the sawtooth, f the number of complete sawtooth cycles in the circle, R_0 base radius of the ratchet profile:

$$S(x) = \begin{cases} 1 - (x \bmod 1) & \text{Spin up} \\ x \bmod 1 & \text{Spin down} \end{cases} \quad (6.14)$$

Points $\mathbf{r} = (x, y, z)$ are included when $\sqrt{x^2 + y^2} \leq R(\phi)$. However, these points must remain fixed, otherwise these would separate from each other dissolving the structure, therefore we add bonds. There are multiple methods to model the potential energy of a bond, the easiest way is to use the harmonic potential that mimics the behavior of a ideal spring and is modeled after Hooke's law:

$$U_{i,j}^H(\vec{x}_{i,j}) = \frac{1}{2}K(\vec{x}_{i,j} - \vec{x}_0)^2, \quad (6.15)$$

where K is the energy per squared distance, $\vec{x}_{i,j}$ is the distance between particle i , and j , and x_0 is the equilibrium distance point.

6.5 System Overview and Workflow

The simulations of this thesis were performed with an open-source software called LAMMPS (Large-scale Atomic/Molecular Massively Parallel Simulator) developed by Sandia National Laboratories. Its advantage is the high efficiency to run simulations in parallel, reducing the time required to perform multiple calculations [111]. We used a modified version of LAMMPS but created custom input scripts using a Python library. These scripts will automate the process of the input scripts that will tell LAMMPS everything about the parameters of our simulation, such as the size of the system, the physical conditions, and how long to run for. After the simulations, we used additional custom scripts with the help of a Python library called Pandas, to analyze the results quickly and efficiently.

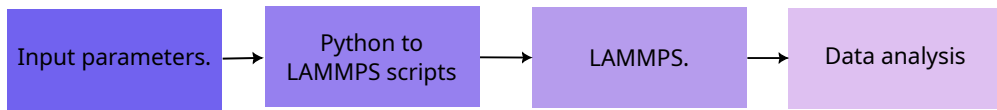


Figure 6.6: Workflow diagram.

6.5.1 System's Physical Definition

The first parameters to be defined are the ones from the circular-ratchet geometry, since it will define the position of the paramagnetic colloids afterwards, these are the parameters that can be specified in the function:

Table 6.1: Parameters used for the circular ratchet in the simulation.

Parameter	Symbol	Ratchet A	Ratchet B	Units
Lattice constant	a	1	1	μm
Radius	r	8	8	μm
Sawtooth amplitude	A	4	4	μm
Sawtooth frequency	N	5	3	Dimensionless
Bond coefficient	K_b	0.1	0.1	μN
Density	ρ	1	1	kgm^{-3}

As shown in the previous table, there were 2 ratchets with only a difference in the *Sawtooth frequency*, but in reality we used a reflection of each ratchet for another pair of analysis. Once the ratchet geometry is defined, then we can define then the remaining of the system, which

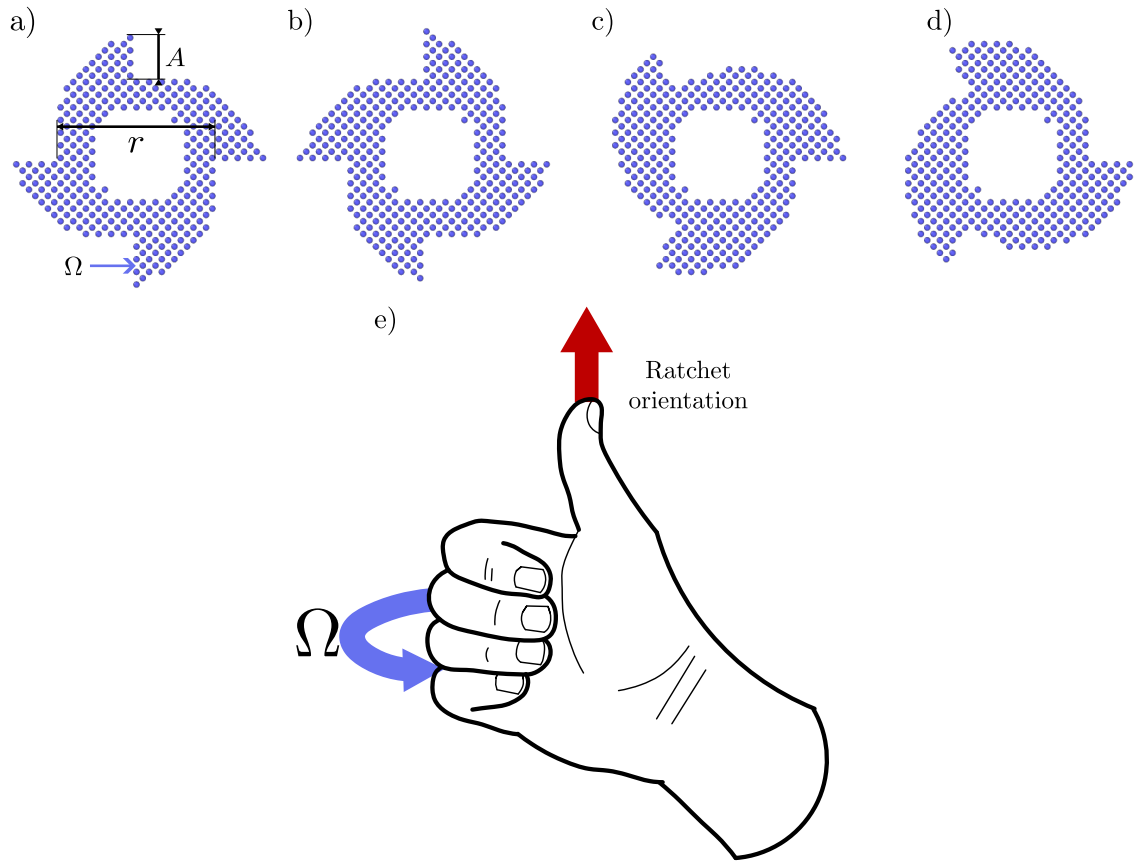


Figure 6.7: Ratchet geometry used in the simulations, a) shows 4-spikes ratchet (Spin up). b) shows the same ratchet with a 180° specular rotation (Spin down). Panel c)- d) Shows the same characterisites with a 3-spikes ratchet. Panel b) Shows the convention used for classifying the ratchets. In this case the curl right hand rule can be used. Facing the “wall” of the ratchet with the palm of the hand, the thumb will indicate the geometry of the ratchet. If the thumb points towards you or upwards, the geometry will be called spin up, if it points downwards the geometry will be called spin down.

remained constant for the 2 ratchets. Starting with the simulation box, that is a rectangle box of periodic boundary conditions in axis x , and y , and finite boundary conditions modeled with the a WCA potential:

Table 6.2: Parameters used for the box of the simulation.

Axis	lo	hi	Units
x	-27	27	μm
y	-27	27	μm
z	-2	2	μm

Where lo represent the lower boundary, an hi the upper boundary.

Finally, the parameters for the paramagnetic particles, and since they deppend on the magnetic field, it is important to define the parameters of this one too.

Table 6.3: Parameters used for the paramagnetic particles.

Parameter	Symbol	Value	Units
Radius	r_{mag}	1.25	μm
Susceptibility	χ	0.4	Dimensionless
Field angle	θ	27	$^{\circ}$
Frequency	f	[0 - 10]	Hz
Field magnitude	B	7.28	mT

With these values, we can run simulations for a period of 50×10^6 frames, with a timestep of $10 \mu s$ which corresponds to a total real time of $500s$ ($8.33\bar{3}min$). Since these systems are of random nature, it is recommended to perform multiple simulations in order to be able to obtain reliable averaged observables, therefore we ran it 10 different times for each frequency.

6.5.2 Data Analysis

When a simulation is completed, LAMMPS generates a text data file containing the quantities selected for output. In this study, we are particularly interested in the particle positions of the solid object, from which several physical properties can be derived—the most relevant being the angular velocity of the ratchet.

The simulated system consists of multiple particles, each exhibiting a slightly different angular velocity due to the bond strength, which prevents them from remaining perfectly rigid with

respect to one another. Consequently, it is necessary to compute an average angular velocity that represents the collective motion of all particles.

Since all particles share the same center of mass, the angular velocity can be determined by first calculating this common center, defined as follows:

$$(x_{\text{COM}}, y_{\text{COM}}) = \frac{\sum_{i=1}^n m_i * r_i}{\sum_{i=1}^n m_i}, \quad (6.16)$$

being m_i the mass of the particle i , and r_i the position of the particle respect a frame of reference. The best way to calculate the angular velocity is by using polar coordinates, once we have the center of mass, we convert the positions to polar coordinates:

$$r_i = \sqrt{(x - x_{\text{COM}})^2 + (y - y_{\text{COM}})^2}, \quad (6.17)$$

$$\theta_i = \arctan \frac{y - y_{\text{COM}}}{x - x_{\text{COM}}}, \quad (6.18)$$

then we can calculate the angular velocity of each particle for each timestep of the simulation:

$$\omega_i = \frac{\Delta\theta_i}{\Delta t}, \quad (6.19)$$

then obtaining an average angular velocity of all particles. We average over all particles to obtain the angular velocity of the solid object.

Part IV

Results

Chapter 7

Results

For the following results, I ran 230 simulations per ratchet, we calculate the mean angular velocity over the different seeds for each frequencies between 0Hz and 10Hz, and to validate the accuracy of each result, we used the error over the mean [112]:

$$\sigma_{\bar{x}} = \frac{\sigma}{\sqrt{n}}.$$

Figure 7.1 summarizes the main result of this work, showing how the average angular frequency of the system changes with the frequency of the rotating magnetic field. At low frequencies (0–3 Hz), the internal dipoles of the paramagnetic colloids can align and rotate in phase with the external field, producing almost no net rotation on the solid ratchet. In this regime, particles are merely diffusive and are stuck in place, not having any displacement overall, which aligns with theoretical expectations. As the frequency increases, the dipoles begin to experience a delay relative to the field rotation. This phase lag and fluid viscosity reduces the alignment efficiency, and the system gradually loses synchronization, observing a phase of neighbours exchange, at this regime the solid ratchet reaches a peak mean angular frequency at 5 Hz. Beyond this critical frequency, the particles no longer move by exchanging neighbors but instead start to experience a repulsion and attraction force between each pair of particles due to not being able to keep up with the field, this behavior resembles that of an harmonic bond. At the same time we observe that the number of teeth on the ratchet’s geometry does not play a significant role in its speed; however, it has a non-negligible impact for the spin up ratchets. Not obstant, this simulation demonstrates how field rotation controls the system’s dynamics.

Figure 7.2 shows the particle trajectories for three representative driving frequencies: 1 Hz, 5 Hz, and 10 Hz. When no field rotation is applied (0 Hz), the particles exhibit random motion dominated by thermal fluctuations, forming a crystalline arrangement that remains largely static and purely diffusive. At 1 Hz, the magnetic moments of the particles follow the external field,

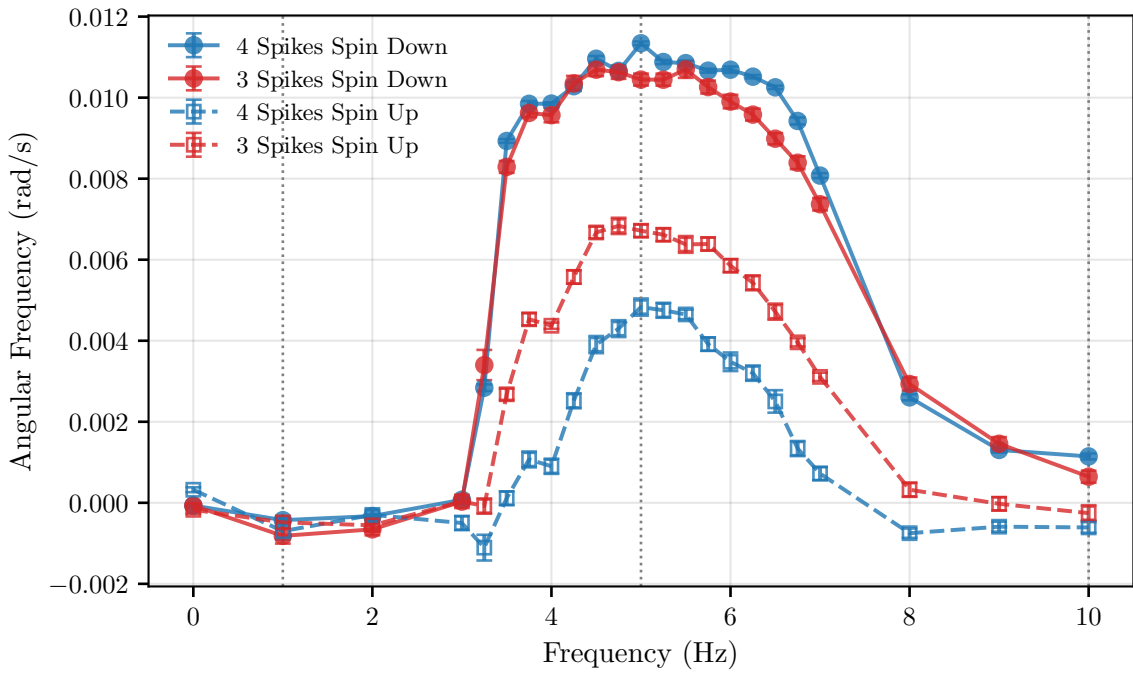


Figure 7.1: Average angular velocity of the paramagnetic colloidal cluster as a function of the rotating magnetic field frequency. Vertical guides at 1, 5, and 10 Hz highlight specific frequency values.

rotating synchronously and forming dimer pairs that spin around a common center of mass while remaining nearly fixed in position. As the frequency increases to 5 Hz, the trajectories become markedly ballistic, indicating that the dipoles are no longer synchronized with the external field and begin to move collectively in a directed manner. Finally, at 10 Hz, the particles appear almost stationary, as the rapid field rotation prevents them from responding effectively. This progression demonstrates that the rotation frequency of the magnetic field governs the transition from random to directed motion. To illustrate this behavior, the trajectory of a single representative particle has been highlighted in each case, clearly showing the rotational motion at 1 Hz, the chaotic displacement at 5 Hz, and the quasi-static behavior at 10 Hz.

Since the angular velocity has very strong fluctuations, a graph over the time will not give us important visual guides whether to determine the properties. Therefore we used a type of convolution known as moving average to obtain a smoother plot. This type of mean focus on a group of values to then ignore them to focus on another new group. According to [113] a two and one sided averages are given respectively by Eq. (7.2), which is, in fact, a low-pass filter, perfect for the large fluctuations.

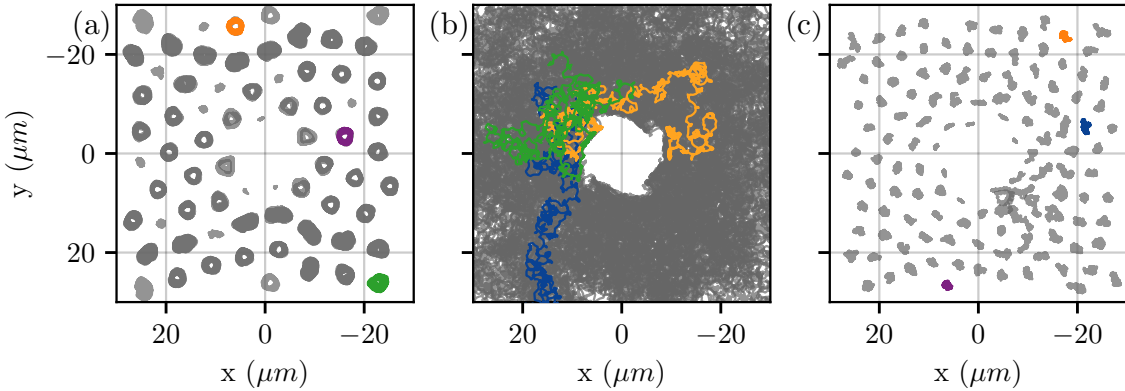


Figure 7.2: Trajectories of the particles of one simulation during the simulation, from 50 - 100 s, for (a) 1 Hz, (b) 5 Hz, and (c) 10 Hz.

$$z_t = \frac{1}{2k+1} \sum_{j=-k}^k y_{t+j}, \quad t = k+1, k+2, \dots, n-k, \quad (7.1)$$

$$z_t = \frac{1}{k+1} \sum_{j=0}^k y_{t-j}, \quad t = k+1, k+2, \dots, n. \quad (7.2)$$

Figure 7.3 presents the time evolution of the angular velocity. At 1 Hz, the system exhibits only random fluctuations caused by thermal noise, with an average angular velocity close to zero. In contrast, at 5 Hz, the angular velocity remains consistently positive over time, despite instantaneous fluctuations. The rolling mean highlights this difference, showing a net rotational trend, although not constant, that reflects the impact the collective behavior colloids have in the rotation of the ratchet.

Due to the inherent variability of stochastic processes, a large amount of data is required to obtain reliable statistics. Figure 7.4 shows the angular velocity histograms for 0 Hz and 5 Hz. Interestingly enough, the data showed a gaussian distribution and to better visualize the shape of the graph, we used a Gaussian Kernel Density Estimation (KDE) to smooth out the histogram [114].

$$\hat{p}_n = \frac{1}{nh^d} \sum_{i=1}^n K\left(\frac{x - X_i}{h}\right) \quad (7.3)$$

$$K(x) = \frac{\exp(-||x||^2/2)}{v_{1,2}}, \quad v_{1,2} = \int \exp(-||x||^2/2) dx. \quad (7.4)$$

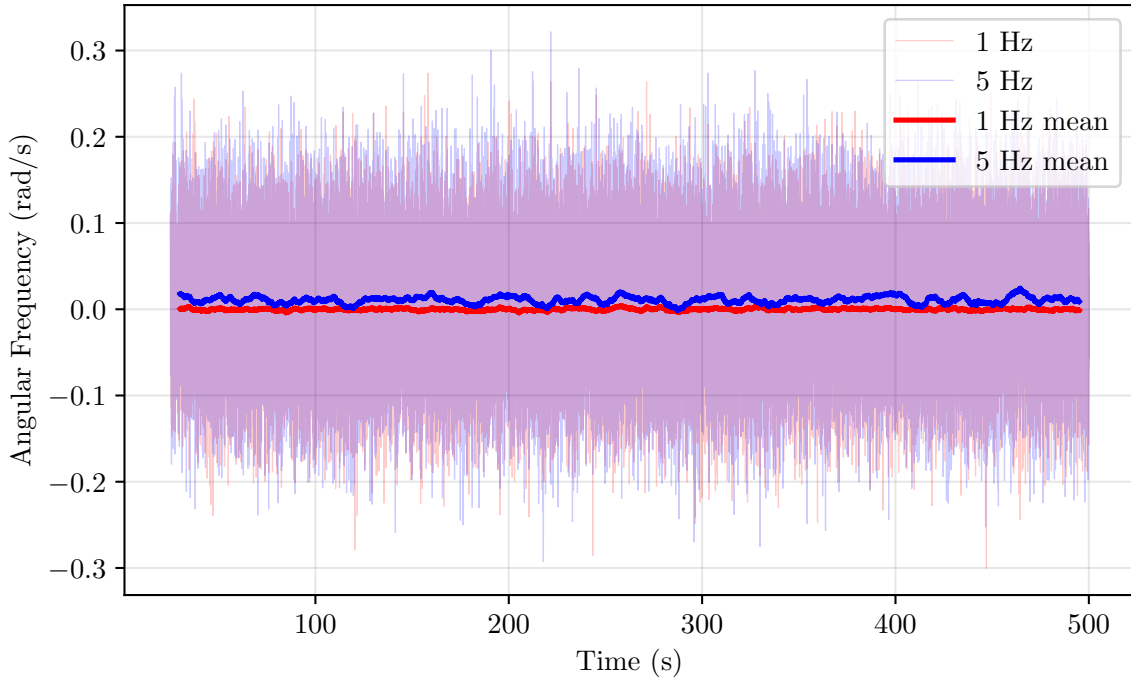


Figure 7.3: Angular velocity of the ratchet as a function of time for a single simulation at 1 Hz and 5 Hz. The shaded regions correspond to the raw data, and the solid lines show the rolling mean.

At 1 Hz, the mean lies almost exactly at 0 rad/s, while the 5 Hz distribution is skewed to the left, indicating a high probability of a positive net rotation and backing up the results of Figure 7.3.

The angular velocity is extremely small, however Figure 7.5 shows the angular displacement of a single ratchet particle over the entire simulation. At 1 Hz, the particle shows an initial displacement but remains largely constant over time, experiencing only thermal fluctuations. This initial displacement can be due to the initial interaction of the closer colloids, which move close to the walls of the ratchet and probably moving or rotating the ratchet a certain, but negligible amount, however, the remaining section is the tendency of not moving for a long period of time. In contrast, at 5 Hz, the particle exhibits a net displacement that appears linear in time, clearly showing a non zero velocity.

To give meaning to the plot, we can obtain the arc length of a circle, this is assuming this as an ideal trajectory for the ratchet, therefore we use the following equation:

$$s = r\theta,$$

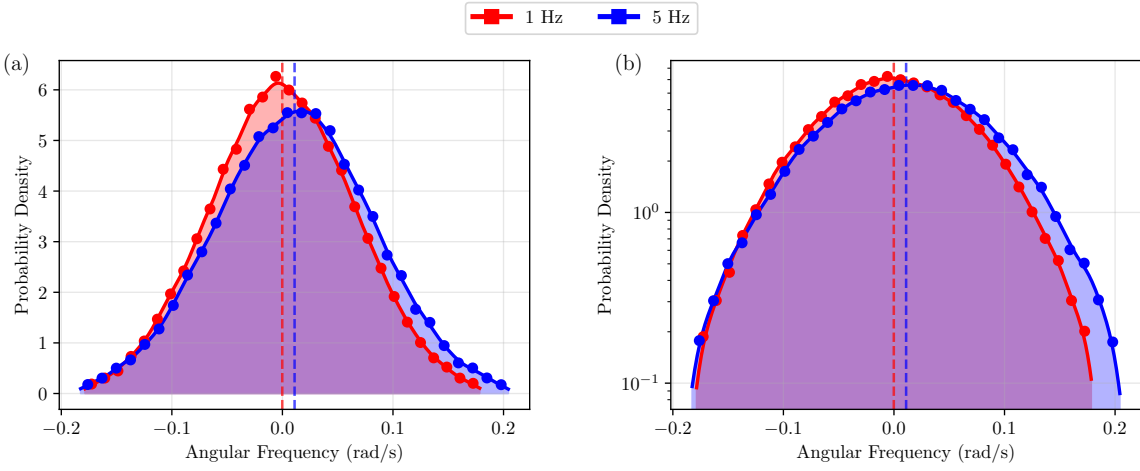


Figure 7.4: Angular frequency distributions for a four-tooth spin-down ratchet obtained from a single simulation. Panel (a) shows the histograms at 1 Hz and 5 Hz, while panel (b) displays the same data on a semilogarithmic scale to emphasize the tails of the distribution.

where s is the arc length, r is the radius of our ratchet and θ is the angle formed from the particle to the initial position. In this case we can see that its final angular position is $\theta \approx 5.5\text{rad}$, which corresponds to the total distance traveled by the particle was $s \approx 44\mu\text{m}$.

In the total simulation, the ratchet experienced a little less than half rotation but more than a quarter, but according to Purcell [1], at those regimes movement not necessarily has to be much. Nevertheless, this provides clear evidence of the frequency's dramatic effect on ratchet rotation. This aligns with the theoretical principle that work cannot be extracted from thermal fluctuations alone. However, we have identified a range of frequencies where colloidal interactions and a driving magnetic field are sufficient to drive ratchet rotation.

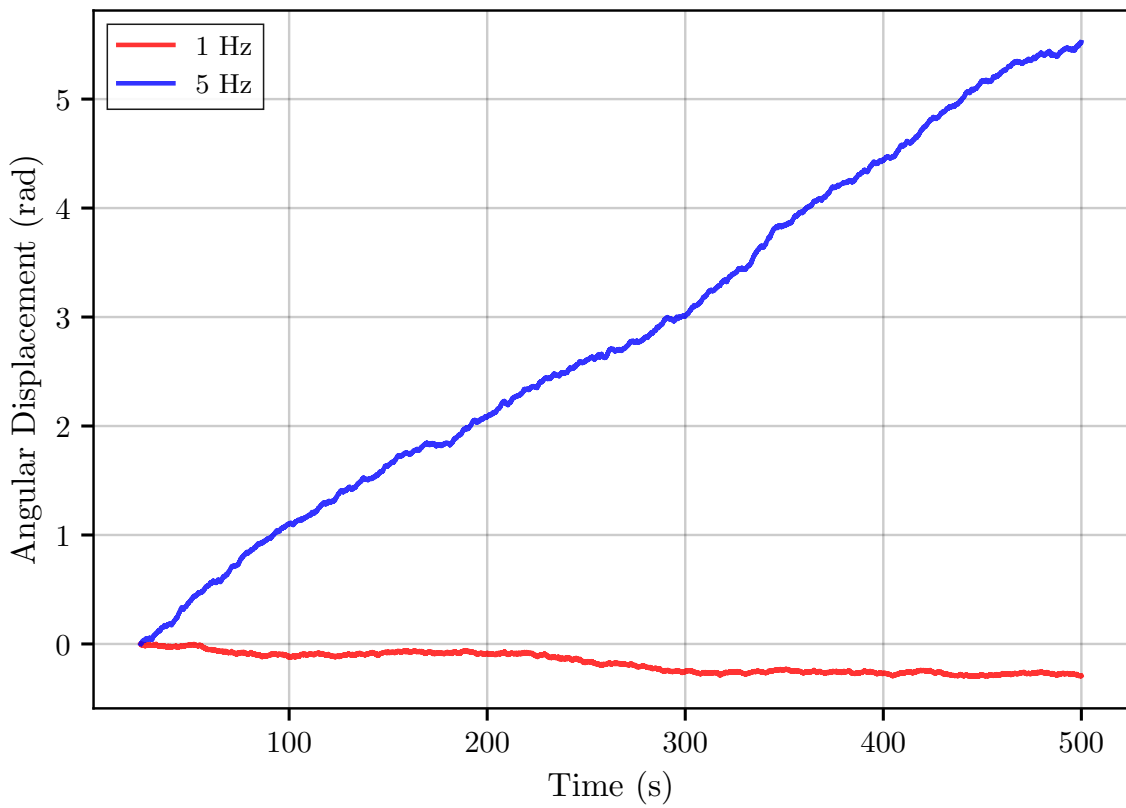


Figure 7.5: Angular displacement of a particle of one simulation at 1 Hz and 5 Hz.

Part V

Conclusions

Chapter 8

Conclusions

We have seen how motion at small scales becomes difficult due to the increase in the relative viscosity of fluids, which suppresses inertia and makes displacement dependent the available degrees of freedom. Random forces, known as thermal fluctuations, also play an important role by constantly disturbing the motion of particles. Nevertheless, both theory and experiments have shown that even passive particles can achieve rectified motion when subjected to specific asymmetric conditions. In this thesis, we focused on ratchet effects, particularly those observed under optically generated potential landscapes.

We also discussed advances in artificial active particles, while emphasizing natural systems. These biological microswimmers demonstrate how energy can be converted into motion and even into useful work, giving rise to micromachines capable of transporting objects or generating rotation through chemical or biological activity. However, these systems face practical limitations: they are prone to biological degradation and require a continuous source of energy to remain active.

As an alternative, we discussed magnetically driven environments, focusing on spherical paramagnetic colloids driven by an external magnetic field. Experimental studies have already demonstrated that it is possible to rectify the motion of such particles, typically using ferrite garnet films to generate the required asymmetry. Yet, there also exist examples where directed motion is achieved without these substrates, relying only on a conical magnetic field.

In this thesis, we explored the effects of a conical external magnetic field on a solid ratchet immersed in paramagnetic spherical colloids suspended in water and confined geometry. The system was studied using Brownian and molecular dynamics simulations. We analyzed physical quantities such as angular displacement and angular velocity, as they are key indicators of motion rectification.

Our analysis suggests that in the frequency range of 3.25–8 Hz there is a noticeable increase

in angular velocity, which remains roughly constant—though with some fluctuations—between 3.75 and 7.75 Hz. This indicates partial rectification of motion. Although the effect is not strong enough to produce complete rotations within short timescales, it opens a new line of research to enhance the efficiency of this type of system. The same behavior was observed for all four ratchet configurations studied. Interestingly, when the ratchet geometry was rotated by 180°, the overall direction of rotation remained unchanged, even though the ratchet walls were mirrored. This raises an open question about whether the rotation can be controlled through geometry or if it depends entirely on the external magnetic field. To ensure the accuracy of these results, we performed additional analyses on individual datasets using a moving mean filter, and histogram for the lowest (0 Hz) and highest (5 Hz) frequencies. These results confirmed the overall behavior observed in the averaged data and validated our main findings.

In summary, we explored how it is possible to obtain work from passive environments when induced in asymmetric potentials in non-symmetric objects. This thesis opens to discussion about how other parameters of the geometry of the ratchet can effectively affect the rotation of it, such as the radius, wall length, a lower or bigger amount of *spikes*, a bigger amount of colloids, different colloids radius.

Bibliography

- [1] Edward M Purcell. Life at low reynolds number. In *Physics and our world: reissue of the proceedings of a symposium in honor of Victor F Weisskopf*, pages 47–67. World Scientific, 2014.
- [2] Albert Einstein. On the theory of the brownian movement. *Ann. Phys*, 19(4):371–381, 1906.
- [3] Jonathon Howard and RL Clark. Mechanics of motor proteins and the cytoskeleton. *Appl. Mech. Rev.*, 55(2):B39–B39, 2002.
- [4] Ronald D Vale. The molecular motor toolbox for intracellular transport. *Cell*, 112(4):467–480, 2003.
- [5] M Cristina Marchetti, Jean-François Joanny, Sriram Ramaswamy, Tanniemola B Liverpool, Jacques Prost, Madan Rao, and R Aditi Simha. Hydrodynamics of soft active matter. *Reviews of modern physics*, 85(3):1143–1189, 2013.
- [6] Sriram Ramaswamy. The mechanics and statistics of active matter. *Annu. Rev. Condens. Matter Phys.*, 1(1):323–345, 2010.
- [7] Daniel Needleman and Zvonimir Dogic. Active matter at the interface between materials science and cell biology. *Nature reviews materials*, 2(9):1–14, 2017.
- [8] Clemens Bechinger, Roberto Di Leonardo, Hartmut Löwen, Charles Reichhardt, Giorgio Volpe, and Giovanni Volpe. Active particles in complex and crowded environments. *Reviews of modern physics*, 88(4):045006, 2016.
- [9] Suraj Shankar, Anton Souslov, Mark J Bowick, M Cristina Marchetti, and Vincenzo Vitelli. Topological active matter. *Nature Reviews Physics*, 4(6):380–398, 2022.
- [10] Frank Jülicher, Armand Ajdari, and Jacques Prost. Modeling molecular motors. *Rev. Mod. Phys.*, 69(4):1269, 1997.

- [11] Peter Reimann. Brownian motors: noisy transport far from equilibrium. *Physics reports*, 361(2-4):57–265, 2002.
- [12] Alessandro Fiasconaro, Werner Ebeling, and Ewa Gudowska-Nowak. Active brownian motion models and applications to ratchets. *Eur. Phys. J. B*, 65(3):403–414, 2008.
- [13] CJ Olson Reichhardt and Charles Reichhardt. Ratchet effects in active matter systems. *Annu. Rev. Conden. Ma. P.*, 8:51–75, 2017.
- [14] Constantin Rein, Martin Kolář, Klaus Kroy, and Viktor Holubec. Force-free and autonomous active brownian ratchets (a). *Europhys. Lett.*, 142(3):31001, 2023.
- [15] Roberto Di Leonardo, Luca Angelani, Dario Dell’Arciprete, Giancarlo Ruocco, Valerio Iebba, Serena Schippa, Maria Pia Conte, Francesco Mecarini, Francesco De Angelis, and Enzo Di Fabrizio. Bacterial ratchet motors. *Proc. Natl. Acad. Sci.*, 107(21):9541–9545, 2010.
- [16] Nicola Pellicciotta, Ojus Satish Bagal, Maria Cristina Cannarsa, Silvio Bianchi, and Roberto Di Leonardo. Wall torque controls propulsion of curved microstructures in bacterial baths. *Phys. Rev. Lett.*, 135(13):138302, 2025.
- [17] Fernando Martinez-Pedrero and Pietro Tierno. Magnetic propulsion of self-assembled colloidal carpets: efficient cargo transport via a conveyor-belt effect. *Phys. Rev. Applied*, 3(5):051003, 2015.
- [18] Pietro Tierno. Depinning and collective dynamics of magnetically driven colloidal monolayers. *Physical review letters*, 109(19):198304, 2012.
- [19] Arthur V Straube and Pietro Tierno. Tunable interactions between paramagnetic colloidal particles driven in a modulated ratchet potential. *Soft Matter*, 10(22):3915–3925, 2014.
- [20] Helena Massana-Cid, Antonio Ortiz-Ambriz, Andrej Vilfan, and Pietro Tierno. Emergent collective colloidal currents generated via exchange dynamics in a broken dimer state. *Sci. Adv.*, 6(10):eaaz2257, 2020.
- [21] Mattia Ostinato, Antonio Ortiz-Ambriz, and Pietro Tierno. Magnetically driven confined colloids: From enhanced diffusion to bidirectional transport. *J. Magn. Magn. Mater.*, 591: 171701, 2024.
- [22] George E Uhlenbeck and Leonard S Ornstein. On the theory of the brownian motion. *Physical review*, 36(5):823, 1930.

- [23] Kerson Huang. *Introduction to statistical physics*. Chapman and Hall/CRC, 2009.
- [24] Richard Phillips Feynman. The feynman lectures on physics. (*No Title*), 1:46, 1963.
- [25] James Clerk Maxwell. *Theory of Heat*. Longmans, Green and Co., London, 1871. The demon first appears in Chapter 22.
- [26] James Clerk Maxwell. Letter to peter guthrie tait, December 11 1867. First mention of the demon concept.
- [27] Léon Brillouin. Maxwell's demon cannot operate: Information and entropy. i. *J. Appl. Phys.*, 22(3):334–337, 1951.
- [28] Rolf Landauer. Irreversibility and heat generation in the computing process. *IBM J. Res. Dev.*, 5(3):183–191, 1961.
- [29] Juan MR Parrondo and Pep Español. Criticism of feynman's analysis of the ratchet as an engine. *Am. J. Phys.*, 64(9):1125–1129, 1996.
- [30] Marcelo O Magnasco. Forced thermal ratchets. *Phys. Rev. Lett.*, 71(10):1477, 1993.
- [31] Ryo Kanada and Kazuo Sasaki. Thermal ratchets with symmetric potentials. *J. Phys. Soc. Jpn.*, 68(12):3759–3762, 1999.
- [32] Armand Ajdari, David Mukamel, Luca Peliti, and Jacques Prost. Rectified motion induced by ac forces in periodic structures. *J. Physique I*, 4(10):1551–1561, 1994.
- [33] Luc P Faucheux, LS Bourdieu, PD Kaplan, and Albert J Libchaber. Optical thermal ratchet. *Physical review letters*, 74(9):1504, 1995.
- [34] Sang-Hyuk Lee, Kosta Ladavac, Marco Polin, and David G Grier. Observation of flux reversal in a symmetric optical thermal ratchet. *Physical review letters*, 94(11):110601, 2005.
- [35] Alejandro V Arzola, Mario Villasante-Barahona, Karen Volke-Sepúlveda, Petr Jákl, and Pavel Zemánek. Omnidirectional transport in fully reconfigurable two dimensional optical ratchets. *Physical review letters*, 118(13):138002, 2017.
- [36] V Lebedev and F Renzoni. Two-dimensional rocking ratchet for cold atoms. *Physical Review A—Atomic, Molecular, and Optical Physics*, 80(2):023422, 2009.

- [37] Julien Deseigne, Olivier Dauchot, and Hugues Chaté. Collective motion of vibrated polar disks. *Physical review letters*, 105(9):098001, 2010.
- [38] Shahin Mobarakabadi, Ehsan Nedaaee Oskooe, Matthias Schröter, and Mehdi Habibi. Granular transport in a horizontally vibrated sawtooth channel. *Physical Review E—Statistical, Nonlinear, and Soft Matter Physics*, 88(4):042201, 2013.
- [39] Alberto Fernandez-Nieves and Ramon Planet. Active and externally driven granular matter, 2022.
- [40] Michael E Cates and Julien Tailleur. Motility-induced phase separation. *Annu. Rev. Condens. Matter Phys.*, 6(1):219–244, 2015.
- [41] Amin Doostmohammadi, Jordi Ignés-Mullol, Julia M Yeomans, and Francesc Sagués. Active nematics. *Nature communications*, 9(1):3246, 2018.
- [42] Tamás Vicsek, András Czirók, Eshel Ben-Jacob, Inon Cohen, and Ofer Shochet. Novel type of phase transition in a system of self-driven particles. *Physical review letters*, 75(6):1226, 1995.
- [43] Hugues Chaté, Francesco Ginelli, Guillaume Grégoire, and Franck Raynaud. Collective motion of self-propelled particles interacting without cohesion. *Physical Review E—Statistical, Nonlinear, and Soft Matter Physics*, 77(4):046113, 2008.
- [44] Paweł Romanczuk, Markus Bär, Werner Ebeling, Benjamin Lindner, and Lutz Schimansky-Geier. Active brownian particles: From individual to collective stochastic dynamics. *Eur. Phys. J. Special Topics*, 202(1):1–162, 2012.
- [45] Jens Elgeti, Roland G Winkler, and Gerhard Gompper. Physics of microswimmers—single particle motion and collective behavior: a review. *Reports on progress in physics*, 78(5):056601, 2015.
- [46] Gerhard Gompper, Roland G Winkler, Thomas Speck, Alexandre Solon, Cesare Nardini, Fernando Peruani, Hartmut Löwen, Ramin Golestanian, U Benjamin Kaupp, Luis Alvarez, et al. The 2020 motile active matter roadmap. *J. Phys. Condens. Matter*, 32(19):193001, 2020.
- [47] Gerhard Gompper, Howard A Stone, Christina Kurzthaler, David Saintillan, Fernando Peruani, Dmitry A Fedosov, Thorsten Auth, Cecile Cottin-Bizonne, Christophe Ybert, Eric Clément, et al. The 2025 motile active matter roadmap. *J. Phys. Condens. Matter*, 37(14):143501, 2025.

- [48] Peter Hänggi and Fabio Marchesoni. Artificial brownian motors: Controlling transport on the nanoscale. *Rev. Mod. Phys.*, 81(1):387–442, 2009.
- [49] Craig W Reynolds. Flocks, herds and schools: A distributed behavioral model. In *Proceedings of the 14th annual conference on Computer graphics and interactive techniques*, pages 25–34, 1987.
- [50] Andrea Cavagna, Irene Giardina, Francesco Ginelli, Thierry Mora, Duccio Piovani, Rafaële Tavarone, and Aleksandra M Walczak. Dynamical maximum entropy approach to flocking. *Phys. Rev. E*, 89(4):042707, 2014.
- [51] Thierry Mora, Aleksandra M Walczak, Lorenzo Del Castello, Francesco Ginelli, Stefania Melillo, Leonardo Parisi, Massimiliano Viale, Andrea Cavagna, and Irene Giardina. Questioning the activity of active matter in natural flocks of birds. *arXiv preprint arXiv:1511.01958*.
- [52] Claudio Carere, Simona Montanino, Flavia Moreschini, Francesca Zoratto, Flavia Chiarotti, Daniela Santucci, and Enrico Alleva. Aerial flocking patterns of wintering starlings, *sturnus vulgaris*, under different predation risk. *Animal behaviour*, 77(1):101–107, 2009.
- [53] Iain D Couzin, Jens Krause, Richard James, Graeme D Ruxton, and Nigel R Franks. Collective memory and spatial sorting in animal groups. *Journal of theoretical biology*, 218(1):1–11, 2002.
- [54] Raphaël Jeanson, Penelope F Kukuk, and Jennifer H Fewell. Emergence of division of labour in halictine bees: contributions of social interactions and behavioural variance. *Animal behaviour*, 70(5):1183–1193, 2005.
- [55] Madeleine Beekman, David JT Sumpter, and Francis LW Ratnieks. Phase transition between disordered and ordered foraging in pharaoh’s ants. *Proc. Natl. Acad. Sci.*, 98(17):9703–9706, 2001.
- [56] J Aguilar, D Monaenkova, V Linevich, W Savoie, B Dutta, H-S Kuan, MD Betterton, MAD Goodisman, and DI Goldman. Collective clog control: Optimizing traffic flow in confined biological and robophysical excavation. *Sci*, 361(6403):672–677, 2018.
- [57] Kolbjørn Tunstrøm, Yael Katz, Christos C Ioannou, Cristián Huepe, Matthew J Lutz, and Iain D Couzin. Collective states, multistability and transitional behavior in schooling fish. *PLoS computational biology*, 9(2):e1002915, 2013.

- [58] Carl Anderson, Guy Theraulaz, and J-L Deneubourg. Self-assemblages in insect societies. *Insectes sociaux*, 49(2):99–110, 2002.
- [59] Michael Tennenbaum, Zhongyang Liu, David Hu, and Alberto Fernandez-Nieves. Mechanics of fire ant aggregations. *Nature materials*, 15(1):54–59, 2016.
- [60] Yael Katz, Kolbjørn Tunstrøm, Christos C Ioannou, Cristián Huepe, and Iain D Couzin. Inferring the structure and dynamics of interactions in schooling fish. *Proc. Natl. Acad. Sci.*, 108(46):18720–18725, 2011.
- [61] Chenchen Huang, Feng Ling, and Eva Kanso. Collective phase transitions in confined fish schools. *Proc. Natl. Acad. Sci.*, 121(44):e2406293121, 2024.
- [62] VV Isaeva. Self-organization in biological systems. *Biol. Bull.+.*, 39(2):110–118, 2012.
- [63] Giorgio Volpe, Sylvain Gigan, and Giovanni Volpe. Simulation of the active brownian motion of a microswimmer. *American journal of physics*, 82(7):659–664, 2014.
- [64] Robert S Cahn, Christopher Ingold, and Vladimir Prelog. Specification of molecular chirality. *Angewandte Chemie International Edition in English*, 5(4):385–415, 1966.
- [65] Prashant Singh and Anupam Kundu. Local time for run and tumble particle. *Phys. Rev. E*, 103(4):042119, 2021.
- [66] Ion Santra, Urna Basu, and Sanjib Sabhapandit. Run-and-tumble particles in two dimensions: Marginal position distributions. *Phys. Rev. E*, 101(6):062120, 2020.
- [67] Massimiliano Semeraro, Antonio Suma, Isabella Petrelli, Francesco Cagnetta, and Giuseppe Gonnella. Work fluctuations in the active ornstein–uhlenbeck particle model. *J. Stat. Mech: Theory Exp.*, 2021(12):123202, 2021.
- [68] José Muñoz-Dorado, Francisco J Marcos-Torres, Elena García-Bravo, Aurelio Moraleda-Muñoz, and Juana Pérez. Myxobacteria: moving, killing, feeding, and surviving together. *Frontiers in microbiology*, 7:781, 2016.
- [69] Rustem F Ismagilov, Alexander Schwartz, Ned Bowden, and George M Whitesides. Autonomous movement and self-assembly. *Angew. Chem. - Int. Ed.*, 41(4):652–654, 2002.
- [70] Walter F Paxton, Kevin C Kistler, Christine C Olmeda, Ayusman Sen, Sarah K St. Angelo, Yanyan Cao, Thomas E Mallouk, Paul E Lammert, and Vincent H Crespi. Catalytic nanomotors: autonomous movement of striped nanorods. *J. Am. Chem. Soc.*, 126(41):13424–13431, 2004.

- [71] Rémi Dreyfus, Jean Baudry, Marcus L Roper, Marc Fermigier, Howard A Stone, and Jérôme Bibette. Microscopic artificial swimmers. *Nat*, 437(7060):862–865, 2005.
- [72] Ambarish Ghosh and Peer Fischer. Controlled propulsion of artificial magnetic nanostructured propellers. *Nano letters*, 9(6):2243–2245, 2009.
- [73] Jonathan R Howse, Richard AL Jones, Anthony J Ryan, Tim Gough, Reza Vafabakhsh, and Ramin Golestanian. Self-motile colloidal particles: from directed propulsion to random walk. *Physical review letters*, 99(4):048102, 2007.
- [74] Jérémie Palacci, Cécile Cottin-Bizonne, Christophe Ybert, and Lydéric Bocquet. Sedimentation and effective temperature of active colloidal suspensions. *Phys. Rev. Lett.*, 105(8):088304, 2010.
- [75] Felix Kummel, Borge Ten Hagen, Raphael Wittkowski, Ivo Buttinoni, Ralf Eichhorn, Giovanni Volpe, Hartmut Löwen, and Clemens Bechinger. Circular motion of asymmetric self-propelling particles. *Physical review letters*, 110(19):198302, 2013.
- [76] Pietro Tierno, Ramin Golestanian, Ignacio Pagonabarraga, and Francesc Sagués. Controlled swimming in confined fluids of magnetically actuated colloidal rotors. *Physical review letters*, 101(21):218304, 2008.
- [77] G Corkidi, B Taboada, CD Wood, A Guerrero, and A Darszon. Tracking sperm in three-dimensions. *Biochemical and biophysical research communications*, 373(1):125–129, 2008.
- [78] M Siva Kumar and P Philominathan. The physics of flagellar motion of e. coli during chemotaxis. *Biophysical reviews*, 2(1):13–20, 2010.
- [79] James G Mitchell, Lynette Pearson, Armando Bonazinga, Simon Dillon, Helen Khouri, and Rosemary Paxinos. Long lag times and high velocities in the motility of natural assemblages of marine bacteria. *Applied and environmental microbiology*, 61(3):877–882, 1995.
- [80] Graeme Lowe, Markus Meister, and Howard C Berg. Rapid rotation of flagellar bundles in swimming bacteria. *Nat*, 325(6105):637–640, 1987.
- [81] Greg M Barbara and James G Mitchell. Marine bacterial organisation around point-like sources of amino acids. *FEMS microbiology ecology*, 43(1):99–109, 2003.

- [82] Greg M Barbara and James G Mitchell. Bacterial tracking of motile algae. *FEMS microbiology ecology*, 44(1):79–87, 2003.
- [83] Raymond E Goldstein. Green algae as model organisms for biological fluid dynamics. *Annual review of fluid mechanics*, 47(1):343–375, 2015.
- [84] P Zhang, S Jana, M Giarra, PP Vlachos, and S Jung. Paramecia swimming in viscous flow. *Eur. Phys. J. Special Topics*, 224(17):3199–3210, 2015.
- [85] Stephen J DeCamp, Gabriel S Redner, Aparna Baskaran, Michael F Hagan, and Zvonimir Dogic. Orientational order of motile defects in active nematics. *Nature materials*, 14(11):1110–1115, 2015.
- [86] Andrey Sokolov, Jaideep Katuri, Juan J de Pablo, and Alexey Snezhko. Synthetic active liquid crystals powered by acoustic waves. *Adv. Mater.*, 37(19):2418846, 2025.
- [87] Peter Friedl, Yael Hegerfeldt, and Miriam Tusch. Collective cell migration in morphogenesis and cancer. *Int. J. Dev. Biol.*, 48(5-6):441–449, 2004.
- [88] Manfred Schliwa and Günther Woehlke. Molecular motors. *Nat*, 422(6933):759–765, 2003.
- [89] Douglas B Weibel, Piotr Garstecki, Declan Ryan, Willow R DiLuzio, Michael Mayer, Jennifer E Seto, and George M Whitesides. Microoxen: Microorganisms to move microscale loads. *Proc. Natl. Acad. Sci.*, 102(34):11963–11967, 2005.
- [90] Rachel R Bennett and Ramin Golestanian. A steering mechanism for phototaxis in chlamydomonas. *J. Roy. Soc. . Interface*, 12(104):20141164, 2015.
- [91] Lidong Qin, Matthew J Banholzer, Xiaoyang Xu, Ling Huang, and Chad A Mirkin. Rational design and synthesis of catalytically driven nanorotors. *J. Am. Chem. Soc.*, 129(48):14870–14871, 2007.
- [92] Luca Angelani and Roberto Di Leonardo. Geometrically biased random walks in bacteria-driven micro-shuttles. *New Journal of physics*, 12(11):113017, 2010.
- [93] Yuichi Hiratsuka, Makoto Miyata, Tetsuya Tada, and Taro QP Uyeda. A microrotary motor powered by bacteria. *Proc. Natl. Acad. Sci.*, 103(37):13618–13623, 2006.
- [94] Sumesh P Thampi, Amin Doostmohammadi, Tyler N Shendruk, Ramin Golestanian, and Julia M Yeomans. Active micromachines: Microfluidics powered by mesoscale turbulence. *Science advances*, 2(7):e1501854, 2016.

- [95] Santiago Muinos-Landin, Alexander Fischer, Viktor Holubec, and Frank Cichos. Reinforcement learning with artificial microswimmers. *Science Robotics*, 6(52):eabd9285, 2021.
- [96] Tal Geva. Magnetic resonance imaging: historical perspective. *Journal of cardiovascular magnetic resonance*, 8(4):573–580, 2006.
- [97] Paul M Matthews and Peter Jezzard. Functional magnetic resonance imaging. *Journal of Neurology, Neurosurgery & Psychiatry*, 75(1):6–12, 2004.
- [98] Roberto Corti and Valentin Fuster. Imaging of atherosclerosis: magnetic resonance imaging. *European heart journal*, 32(14):1709–1719, 2011.
- [99] Nicole Pamme. Magnetism and microfluidics. *Lab Chip*, 6(1):24–38, 2006.
- [100] Helena Massana-Cid, Fanlong Meng, Daiki Matsunaga, Ramin Golestanian, and Pietro Tierno. Tunable self-healing of magnetically propelling colloidal carpets. *Nature communications*, 10(1):2444, 2019.
- [101] Arthur V Straube and Pietro Tierno. Synchronous vs. asynchronous transport of a paramagnetic particle in a modulated ratchet potential. *Europhys. Lett.*, 103(2):28001, 2013.
- [102] Ralph L Stoop, Arthur V Straube, Tom H Johansen, and Pietro Tierno. Collective directional locking of colloidal monolayers on a periodic substrate. *Phys. Rev. Lett.*, 124(5):058002, 2020.
- [103] N Osterman, D Babić, I Poberaj, J Dobnikar, and P Ziherl. Observation of condensed phases of quasiplanar core-softened colloids. *Physical review letters*, 99(24):248301, 2007.
- [104] Fanlong Meng, Antonio Ortiz-Ambriz, Helena Massana-Cid, Andrej Vilfan, Ramin Golestanian, and Pietro Tierno. Field synchronized bidirectional current in confined driven colloids. *Phys. Rev. Research*, 2(1):012025, 2020.
- [105] Scott J Erickson, RW Prost, and ME Timins. The “magic angle” effect: background physics and clinical relevance. *Radiology*, 188(1):23–25, 1993.
- [106] Jacek W Hennel and Jacek Klinowski. Magic-angle spinning: a historical perspective. *New techniques in solid-state NMR*, pages 1–14, 2004.

- [107] Kar W Yung, Peter B Landecker, and Daniel D Villani. An analytic solution for the force between two magnetic dipoles. *Physical Separation in Science and Engineering*, 9(1):39–52, 1998.
- [108] Siegfried Hess. Augmented van der waals equation of state for the lennard-jones fluid. *Physica A*, 267(1-2):58–70, 1999.
- [109] Eckhard Platen and Nicola Bruti-Liberati. *Numerical solution of stochastic differential equations with jumps in finance*, volume 64. Springer Science & Business Media, 2010.
- [110] Desmond J Higham. An algorithmic introduction to numerical simulation of stochastic differential equations. *SIAM review*, 43(3):525–546, 2001.
- [111] A. P. Thompson, H. M. Aktulga, R. Berger, D. S. Bolintineanu, W. M. Brown, P. S. Crozier, P. J. in ’t Veld, A. Kohlmeyer, S. G. Moore, T. D. Nguyen, R. Shan, M. J. Stevens, J. Tranchida, C. Trott, and S. J. Plimpton. LAMMPS - a flexible simulation tool for particle-based materials modeling at the atomic, meso, and continuum scales. *Comp. Phys. Comm.*, 271:108171, 2022. doi: 10.1016/j.cpc.2021.108171.
- [112] Douglas G Altman and J Martin Bland. Standard deviations and standard errors. *Bmj*, 331(7521):903, 2005.
- [113] Rob J Hyndman. Moving averages. In *International encyclopedia of statistical science*, pages 1559–1562. Springer, 2025.
- [114] Yen-Chi Chen. A tutorial on kernel density estimation and recent advances. *Biostatistics & Epidemiology*, 1(1):161–187, 2017.

Curriculum Vitae

Yeray Cruz Ruiz was born in Tlalnepantla, Estado de México, México. He received a Bachelor of Science degree in Mechatronics (2021) from Tecnológico de Monterrey, Campus Estado de México, México, and is currently a full-time master's student in Nanotechnology, in Tecnológico de Monterrey, Campus Monterrey, focusing on computational studies of soft matter systems out of thermodynamic equilibrium. His research interests include Soft Matter Physics, Colloidal Models, Passive Matter, Active Matter, and Computational Physics.